Electronic Theses and Dissertations, 2004-2019

2012

Numerical Study On Reinforcement Mechanism Of Copper/carbon Nanotubes Composite

Xiang Long
University of Central Florida

NUMERICAL STUDY ON REINFORCEMENT MECHANISM OF
COPPER/CARBON NANOTUBES COMPOSITE

by

XIANG LONG
B.S. Shanghai Jiaotong University, 2002
M.S. Shanghai Jiaotong University, 2005

A thesis submitted in partial fulfillment of the requirements
for the degree of Master of Science
in the Department of Mechanical, Materials and Aerospace Engineering
in the College of Engineering and Computer science
at the University of Central Florida
Orlando, Florida

Spring Term
2012

Major Professor: Yuanli Bai

ABSTRACT

Because of its high stiffness, carbon nanotubes (CNTs) are considered as one of the widely used reinforcement materials in the metal matrix composites. In this thesis, finite element (FE) models were built in Ls-Dyna3D to simulate Copper/CNTs composite deformation and fracture, and to explore CNTs reinforcement mechanisms. Several possible mechanisms were discussed.

Deformation and failure of Cu/CNT composites were studied numerically using unit cell FE models, which consist of both metal matrix and CNTs. The simulation results have been verified by existing experiment data reported by Chen's group. The matrix material was modeled as elasto-plastic ductile solids. The CNTs material properties were taken from literature results using molecular dynamics simulation. FE simulations have showed that CNTs deformation exceeds material elastic limit, which means that CNTs plasticity should be taken into account as well. 2D unit cell models were developed using axial symmetric elements with suitable boundary conditions. Several mechanisms are found to affect CNTs reinforcement prediction. The first one is the boundary condition imposed in the models. The CNTs significantly affect the plastic flow of copper during plastic deformation, which is one important reinforcement mechanism. The second reinforcement mechanism is found to be the hardening zone of Cu matrix around CNTs, which is introduced by mismatch of coefficient of thermal expansion (CTE).

A round of parametric studies was performed to investigate the effects of several modeling parameters in the FE simulations; these parameters include the volume fraction of CNTs, aspect ratio of CNTs, the size of hardening zone, and the residual plastic strain in the zone.

A tool combining Matlab and Ls-Dyna was developed to automatically build 2D unit cell models and automatically post-process simulation results. Picking up suitable parameters, 2D unit cell model results well predict the experimental results from Chen's group. It should be noted that the interface between Cu and CNTs was assumed to be perfect in FE simulations since no CNTs debonding was observed in the experiments.

Also, a 3D unit cell model using tetrahedral elements (with element numbers up to one million) was tentatively developed to obtain more accurate results. The purpose was to explore the interface properties of Cu/CNTs, the effect of CNTs orientation distribution, and the other reinforcement mechanism coming from geometry necessary dislocation (GND) since the size of Cu matrix is divided into nano scales by CNTs. 3D unit models are also used to verify the 2D unit cell one, which is a simplified and effective approach. Very interesting results was observed in this part of study. Further works are needed to overcome the difficulties in 3D modeling and the limitation of current CPU speed.

ACKNOWLEDGMENTS

TABLE OF CONTENTS

LIST OF FIGURES

LIST OF TABLES

CHAPTER 1: INTRODUCTION

Carbon nanotubes(CNTs)[1-3] is regarded as one of the stiffest and strongest materials ever discovered. Because of CNTs' such outstanding characteristics, CNTs have received considerable interest in research. New technologies developed to synthesis MWCNTs and SWCNTs reinforced metal matrix material greatly, these advances make it feasible to develop new carbon nanotubes composites material. CNT reinforcement technologies are used in many fields, copper/CNT composites improved thermal expansion, thermal and electrical conductivity of electric motors brushes[4], Cha et al's studies show that CNT effectively reinforces copper strength[5], and lowers wear rates and friction coefficients[6]. Thus, develop new carbon nanotubes composites to improve material properties has become an interesting research area [5-8].

Theoretical models and experimental measurements have implemented to study the mechanism of deformation, fracture and predict composite material behavior under complex conditions[9]. Some studies focus on the mechanism of CNTs and its Metal-matrix composites [5] behavior under complex conditions; some researches focus on molecular level, molecular structural mechanics model[10] is a simplified elastic model, molecular dynamics[11, 12] simulate elastic and plastic process during tensile process, these two method are useful in predicting nano-composites behavior in microscope, but these models are not feasible to predict material in macroscopic scale calculation because of limitation of computer capacity. Continuum mechanics model is a feasible way[9] to study CNTs composites in microscope under complex stress conditions.

To build up theoretical models in actual application, one thing need to be addressed is the transition from CNTs to metals matrix, this transition area is generated during manufacture process, such as thermal expansion difference [13, 14], heterogeneous plastic deformation[15] and phase transformation[15]. Residual stress arises during manufacture period, which provide additional stiffness. Most of composite materials have this transition area. The characteristics of this area are totally different CNTs and metal matrix [16, 17] which plays key roles to change metal matrix stress strain properties. Simplified two parts models [5, 9] cannot accurately explain the whole tensile process. Nano-composites behavior changed much due to transition part between CNTs and metal matrix. Thus, considering transition part between is important to build up an accurate theoretical model.

With the experiment data of pure metal under different stress condition, and molecule dynamics calculation of CNTs, elasticity of CNTs metal matrix composites can be obtained. After comparing the CNTs composites experiment results with finite element model calculation, modification and adjustment can be made until model calculation results fits experiment result. The major parameters to compare is the stress-strain curve, if two stress-strain curves fits each other, we can say that the finite element model can predict CNTs composites behavior.

To deal with strain softening and incorrect convergence when the element is refine to vanishing size in our calculation, nonlocal damage theory is applied[18]. Base on nonlocal damage theories, the failure criterion is depends on the status of material within a radius around the integration points. An obvious advantage of nonlocal failure is that it can greatly reduce mesh size effect on failure. The only required modification in calculation is to replace the usual local damage energy with its spatial average over the representative volume of the material whose size

2

is a characteristic of the material. The key idea of the nonlocal damage theory is to subject to nonlocal treatment only those variables that control strain softening, and to treat the elastic part of the strain as local [19].

In this thesis, we study the mechanism of harding and failure of CNTs nano-composites. We fit a stress-strain curve and failure criterion base on constant-fracture strain model, with this model we can precisely predict nano-composites material behavior under complex tensile conditions. The failure criterion is obtained through numerical iterations, and model is validated by means of experiment. This paper summarizes mechanisms of hardening of CNTs copper composites, and provides a feasible procedure to study nano-composites characteristics.

CHAPTER 2: LITERATURE REVIEW

2.1 Carbon-nanotube composites

The motivation from the automobile and aerospace to develop light and high strength materials has been recognized, as these properties of material improved, fuel economical of transportation can be improved greatly. Since pure metals and alloys cannot provide enough strength and stiffness, developing metal matrix composites is one of the best ways to solve this dilemma, metal matrix provides strength and ductility, and stiffness is by reinforced high stiffness material, such as CNTs. Due to high Young's modulus, high strength with low density, high toughness and flexibility of carbon nano-tubes[20-22], synthesis of CNTs is a feasible way to improve material properties, such as carbon nantotube-polymer composites[23, 24], metal matrix composites[25-27].

CNTs extraordinary mechanical properties are showed in numerous experiments and simulations, such as extremely high Young's modulus 0.5-150 TPa[28-35], large ultimate tensile strengths range from 20GPa to 150 GPa[28, 34-36], very high flexibility[37], and thermal conductivity up to $600W^{-1}K^{-1}$[38, 39]. The excellent CNTs mechanical properties are because of high bond strength of carbon-carbon bonds and perfect lattice structure[40].

Recent years, people carried out a lot of research about CNTs reinforcement in materials, such as polymer and metals. Figure 1 shows the statics of journal papers published recent years on CNT composites. From the statics, most of CNT reinforced matrix studies have been carried out on polymer base materials, whereas the major structural materials applications today are metals. Figure 2 shows the number of publications on CNT-metal matrix each year. From Figure 2, we can say that obviously increased papers published after 2003.

4
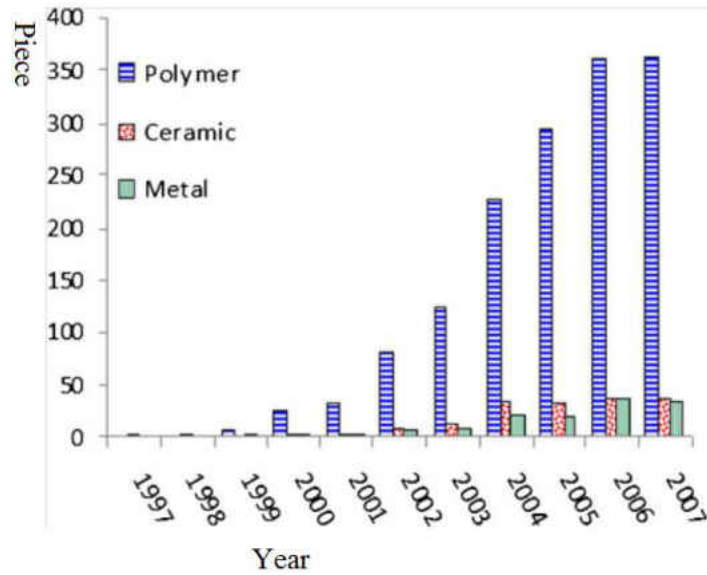
Figure 1 statics of CNT composites reinforced materials
(source:www.scopus.com)[41]
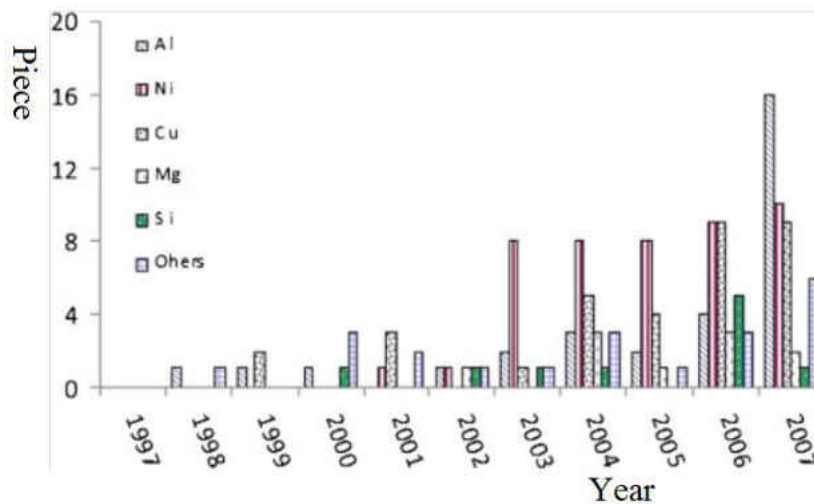
Figure 2 Statics of papers on different metal matrix base CNT composites
(Source: www.scopus.com[41])

CNT composite reinforcement is widely used to improve polymer properties. Some

reviewed papers presented on polymer base CNTs composites [42-48], and different resins [49,

5

50]. Some papers addressed the problems for ceramic matrix composites [51-53]. Jia et al.[23] prepared nanocomposites with situ polymerization of poly (PMMA) and MWNTs, the mechanical properties are improved greatly due to very high interfacial strengths in between CNTs and polymers. Haggenmueller's[48] study showed that orientation of nanotubes significantly influence nanocomposites properties. Zhou et al[54]. did a comprehensive studies on anisotropic distribution of MWNTs in polymer, the alignment of carbon-nanotubes in the composites showed that the degree of alignment is critical for anisotropic properties of CNTs, and degree of alignment can be controlled by stretching ratio.

To fabricate metal/CNT composites, many techniques are reported[41] to prepare it. Powder metallurgy is the most popular and widely technique to fabricate metal matrix CNTs composites. electroless and Electrodeposition [41] deposition are another important techniques, which is next to powder metallurgy, to fabricate metal matrix CNT composites. For low-melting-point metals such as Mg and bulk metallic glasses[41], melting and solidification is a viable solution. Except these techniques, other routes have been developed to fabricate metal matrix CNT composites. The techniques are presented in the following section.

2.2 Carbon-nanotube composites processing techniques

One of the most important issues to prepare CNT metal matrix composite is the CNTs dispersion in composites, the main purpose of many research and experiments is to improve it. Another issue need to be considered is the reinforcement of CNTs, which depend on the interfacial wettability between CNTs and metal matrix. Also chemical reaction should be avoided during composites manufacture process.
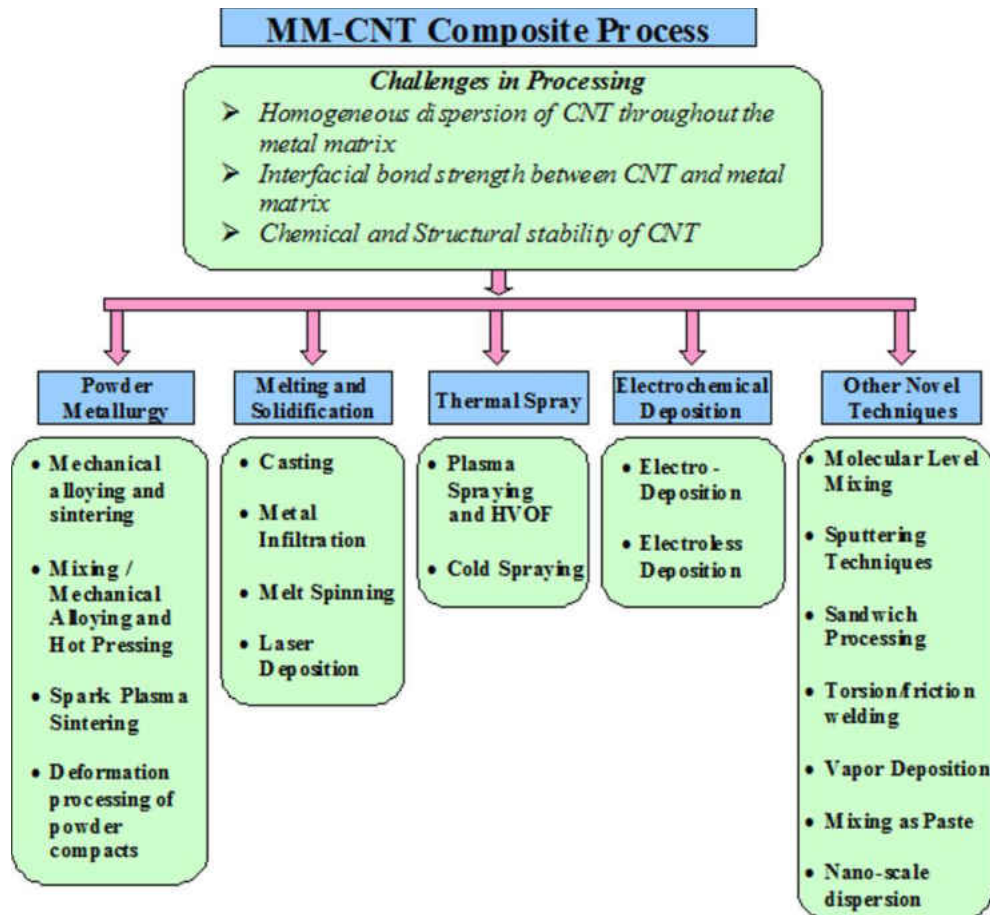
Figure 3 Metal matrix CNTs composite processing
Several metal matrix CNT composites methods are presented[41]

Many ways have already been studied to manufacture metal matrix nano-composites [41]:

1.   Power metallurgy;

2.   Melting and solidification;

3.   Thermal spray;

4.   Electro chemical deposition;

5.   Other novel techniques.

An overall disgram is showed in Figure 3 about metal matrix CNTs composites processing.

The common challenges in these processing technologies are:

1. CNT homogeneous dispersion in metal matrix;

2. Bond strength at the interface between CNT and metal matrix;

3. Stability of CNTs inside metal matrix.

2.2.1 Powder metallurgy

Mechanical alloying and sintering

Power metallurgy technology is widely used, especially in Cu/CNT and Al/CNT composites studies, and a few Sn, Ag, Ni, Ti, Mg matrix base CNT reinforced composites. Some metal matrix nano-composites such as Cu-CNT[6, 55], Al-CNT[56], W-Cu[57] and Ag-CNT[58], are prepared with mechanical alloying and sintering.

Mixing/mechanical alloying and hot pressing

Hot pressing is another way researcher to consolidate powder mixtures. Since some studies showed that it is inappropriate to fabricate AL-CNT composites because of CNT clustering [59, 60]. Dent et al. [61] electroless coat Ni on CNTs which address dispersing problems, Kuaumaki et al. [62] avoid CNTs damage and prepare Ti-CNT composite by hot pressing after 5 hours mechanical mixing, Carreño-Morelli et al.[63] and Pang et al.[64] improved mechanical properties through uniform dispersing of CNTs.

Spark plasma sintering

Spark plasma sintering(SPS) is a process which a pulsed direct current is passed through a die and the powder, producing rapid heating and then enhance the sintering rate greatly[41, 65]. This produced saved time on grain growth to consolidate nano powder. The method is mainly applied to produce Cu-CNT[5, 66, 67], Al-CNT composites[68].

Deformation processing of powder compacts

To improve CNTs density, distribution and alignment in composites, some researcher tried to deform composites powder compacts. Kuzumaki et al.[69] achieve better alignment in the Al-CNT composites through hot powder compact extrusion at 873K. However, this approach is limited to Cu-CNT [70-72] and Al-CNT [73-79] composites.

2.2.2 Melting and solidification procedure

This method is only feasible for low melting point metal, because CNTs may burns under high temperature, or react with metal matrix at the CNT/metal interface. The sub-routine of this method include: casting, metal infiltration, melt spinning and laser deposition.

Bian et al.[80, 81] produced Zr base metal CNT composites by casting, which enhanced hardness and also crystallinity at the same time because of CNT reinforcement. There is also Mg-CNT [82, 83] composites research reported after melting and casting, due to low melting point of Mg.

There is also research reported with infiltration method to disperse CNTs in composite. This process is to disperse CNTs inside porous medium, then infiltrate liquidized metal into porous medium to produce composite structure[41]. Mg-CNT[84] and Al-CNT[85] metal matrix composites are reported, the metal matrix is well reinforced, and the hardness and wear resistance of composites are well improved. Li et al.[86] reported CNT-$Fe_{82}P_{18}$ metallic glass composites through pouring molten alloy on to a rotating CU wheel, the alloy is cooled rapidly which generate metallic composite ribbons[41]. Ni-CNT composite is prepared through laser deposition by Huwang el al[87].

2.2.3 Electrochemical procedure

Electrochemical procedure is the second popular method after power metallurgy techniques [41] based on the number of metal matrix CNT composites publications, Electro deposition and electroless-deposition are two major sub-index.

It is reported that electro deposition is mainly used to prepare Ni-CNT [88-102] and Cu-CNT matrix composites [103-106]. Recently, many researches are reported to plating techniques are employed to prepare metal/CNT composites [89, 91, 93, 99, 107-111]. Arai [112] fabricated CU/CNT composites plating by pulse-reverse (PR) electro-deposition method was investigated in order to increase MWCNT content of the composite plating files. To determine the best current in electro-deposition process, electron microscopy and X-ray diffraction were employed to investigate the electro-deposition and dissolution behaviors of composite films. It is reported from the previous studies, that the higher CNT concentration of electrolyte, current density and agitation rate of bath, the higher CNT vol fraction.[92, 93]. Electroless deposition, which is first reported by Chen et al.[113], is the process of depositing a coating with the aid of a chemical reducing agent in solution, and without the application of external electrical power. A few CNT metal matrix composites, Co-CNT[56], Ni-Fe-P[66] alloy and Ni-Cu-P[114] alloy have been fabricated using this approach.

2.2.4 Other processing technique

Thermal spray is another efficient manner to incorporate CNTs into coatings and bulk components. Better wear resistance and thermal conductivity of the composites in the studies. The major advantage of thermal spraying is to provide large cooling rate, which can reach $10^8 K^{-1}$

in solidification process [115-117]. Thermal spray can be classified into three sub-methods: flame spraying, cold spraying, high velocity oxy-fuel spraying and plasma spraying [41].

Except the method mentioned above, some other methods also reported, which are not widely used, such as Cu-CNT composites[5, 67, 118, 119] with molecular level mixing, sputtering route[120, 121].

2.3 Nonlocal theory

Nonlocal method has been considered as an efficiently computation method to deal with the defects come with incontunuum medium in softening. The material damage behavior under force have been elaborated by many theories, such as coalescence, nucleation and micro-defects [122]. As a certain damage point is attained, damage result to degradation of material elasticity and remarkable overall strength reduction. The latter phenomenon is strain softening, which is considered as the computational and theoretical difficulties in continuum structural model.

Some regulation techniques are carried out to overcome the shortcomings that mentioned above, the most simple one is the fracture energy regularization approach [123-125]. This approach is efficient and simple, but it does not provide spatial band damage distribution in the model. Nonlocal approaches are carried out, which comes with clear micro-mechanical interpretations. Nonlocal approaches are defined in two forms, one is strong form(spatial integral)[126-129], the other one is weak form(spatial higher gradients)[130-134].

Polizzotto [135] and Borino [128] developed nonlocal damage problems base on a nonlocal dissipative problems. This approach is extended to strain-softening plasticity which is

originated from thermodynamic format. Benvenuti et al.[136] consider nonlocal approach as the damage-hardening internal variable.

2.4 Residual stress&strain in metal matrix CNT composites

There is one thing must be considered in metal matrix CNT composites, the transition part between CNTs and metal matrix. Usually the transition parts contain residual strain/stress during manufacture process, which play key roles in improving composites characteristics.

Chemical and complex temperature cycles are applied in forming process to fabricate metal matrix CNTs composites. Complex chemical and thermal reaction during the cycles within the composites produce internal stress which come from different sources, such as unmatched thermal expansion [137].

Plastic residual strain mechanism is studied by Suh et al. [17] and Arsenault and Shi[138]; in their studies, plastic residual strain is produced by coefficient of thermal expansion(CTE) and elastic-plastic mismatch at the interface of reinforcement particle and matrix, additional stress is generated by the residual strain, which is called residual stress. A model is developed to predict plastic dislocation around the particles by Arsenault and Shi [138], the calculation result showed that mismatch thermal expansion [14] produce plastic strain because of the geometrically of dislocation(GND). Strain gradients are also generated a the interface of particle-matrix by elastic-plastic mismatch which comes with deformation also generate GNDs [139], but the dimension of yield strength result from this process is obviously smaller than that produced in the CTE process.

Due to the elastic-plastic mismatch between the particle and matrix, plastic strain gradients are also produce GNDs[139] which come with deformation, while yield strength is reinforced smaller by this process than that generated by CTE mismatch[140].

Figure 4 [17] give a brief idea GND micro-structure. Figure 5 illustrate discrete particle distribution in composites, every particle is surrounded by a hardened area which contains additional residual stress, the strength of the composites is influenced by this are greatly.
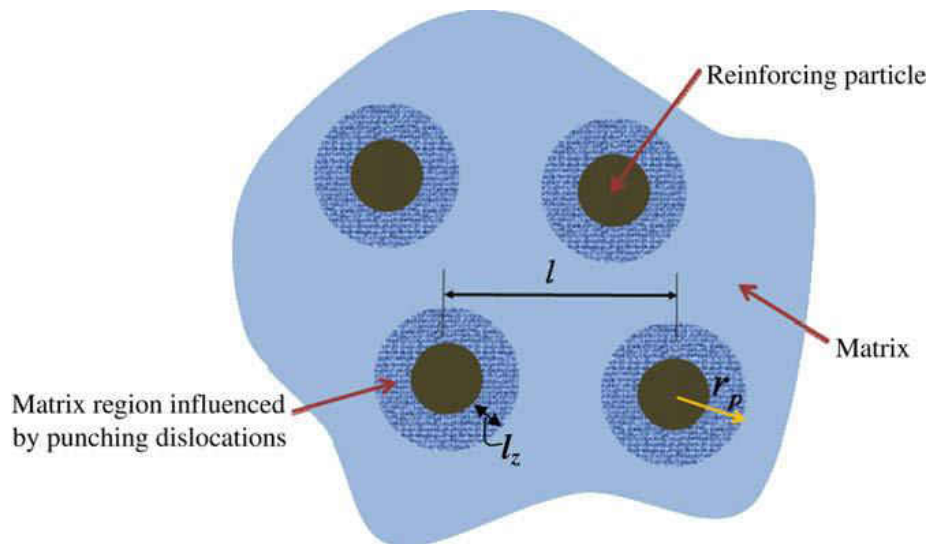
Figure 4 punched area distribution around each particle [17]

Volinsky et al. [13] studied microstructure of electroplated copper film on different barrier layers and residual stress inside this films, Rozeveld et al. [141] measured the residual strain in Al-SiCw composites with convergent-beam electron diffraction, Yin et al,[142] measured the residual strains associated with the curing process to fully understand how the woven structures behave after cure.

Several methods were employed to determine the residual strains in composite materials, Sicot et al.[137] and Wu et al.[143] employed hole-drilling method to measure residual stress in

composites materials; Thermal residual stress among different laminar in woven graphite composites is studied by Benedikt et *al*.[144]; Zewi et al.[145] measured residual stress in woven glass epoxy laminates; and several analytical model are employed a combination of modified classical laminate theories and finite element modeling[146].

CHAPTER 3 EXPERIMENT

3.1 Uniaxial tensile test

In this thesis, our research is mainly focus on FEA modeling and simulation. All experiments are carried out by Dr Chen etc *al*.[147]. Then FEA models are evaluated base on these experiment data. In this chapter, I will introduce simplified experiment procedure which carried out by Dr Chen etc *al*.[147].

The fabrication of Cu/CNT nanocomposites is prepared by an innovative electrochemical co-deposition, which is developed and finished in Dr Chen's lab[147], in this process the CNTs can be driven and deposited onto a cathode, together with copper ions. CNTs are dispersed in the copper electrolyte and both CNTs and copper ions are deposited on the cathode at the same time during deposition reaction. Therefore, uniform CNT distribution in the copper matrix has been manufactured (Figure 5). Figure 5 shows CNTs dispersed well in composites.

Figure 5 SEM picture of Cu/CNT composites
 Composites is fabricated by the electrochemical co-deposition[147]

To determine mechanical properties of Cu/CNT nanocomposites, Cu/CNT samples are prepared in a dog-bone shape by UV-LIGA process (Figure 6). In fabrication process, a thin copper layer is deposited first on a silicon wafer by a physical vaporization process. This thin Cu layer is used as seed layer for Cu/CNT electrochemical deposition. Su-8 molds are used to define the shape and size of tensile test sample Figure 7(a). In order to compare CNT reinforcement effect on pure copper, pure copper sample without CNTs is also prepared by the same procedure.

The thickness of samples is controlled by deposition time, and measured by electron microscopy (SEM) scanning; the shape is predetermined by the molds, which is showed in Figure 6. Tensile tests were carried out with a Tytron 250 Microforce Tester System (MTS, USA)[147]. The tested samples are examined under microscope scale (Figure 7(b)). After test, deposit and fractured surface are studied using TEM and SEM (JOEL 6400F).

(a)   (b)
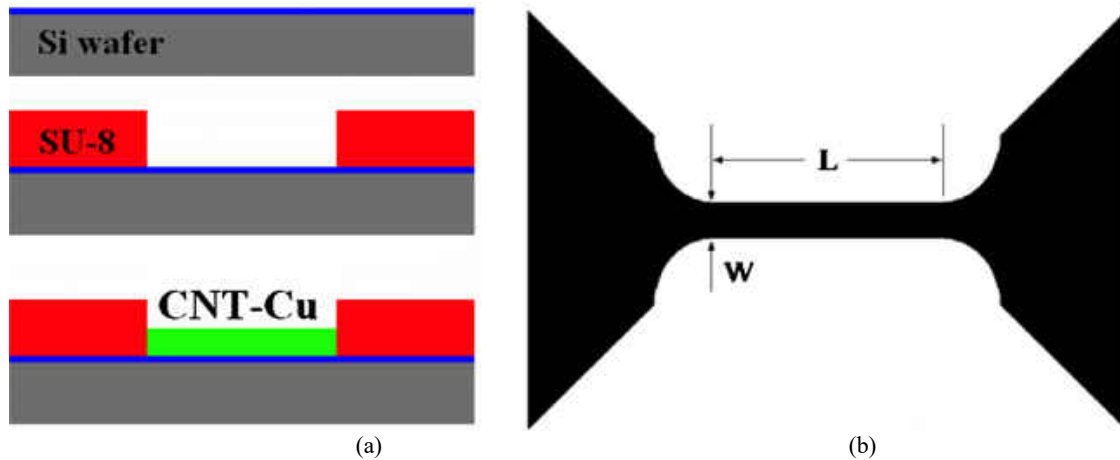
Figure 6 top view of a dog-bone shape CU tensile test sample[147]

(a)   (b)
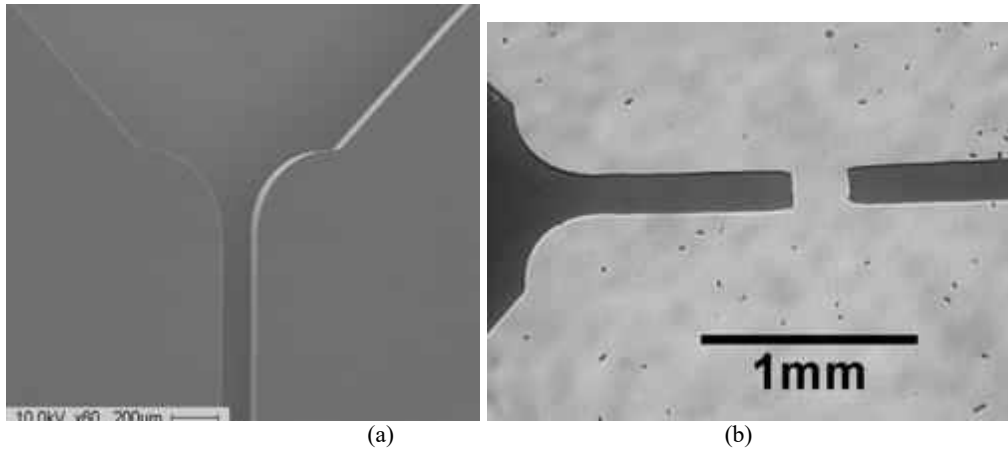
Figure 7(a) SU-8 fabrication mold SEM image. (b) A fractured sample image (copper CNT composites) after tensile test[147].

3.2 Experiment result

Figure 8 shows a stress-strain curve comparison of Cu/CNT nanocomposite and pure copper. Figure 8 indicates that electrochemically deposited copper can reach a yield stress as high as 75MPa (0.2% offset strain) and an ultimate tensile strength of 230 MPa. The strength data are comparable to the published data[147]. According to Figure 8, the yield strength of CNTs reinforced copper can reach 420 MPa, which is about five times larger than that of pure copper.
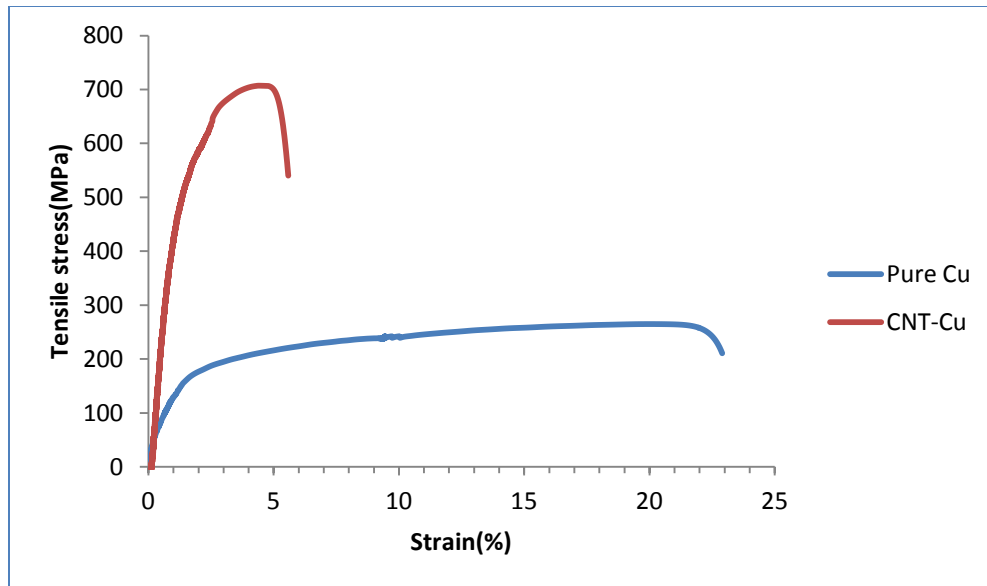
Figure 8 A typical engineering tensile stress-strain curves
Comparison between Cu/CNT nanocomposite sample and pure Cu sample[147]
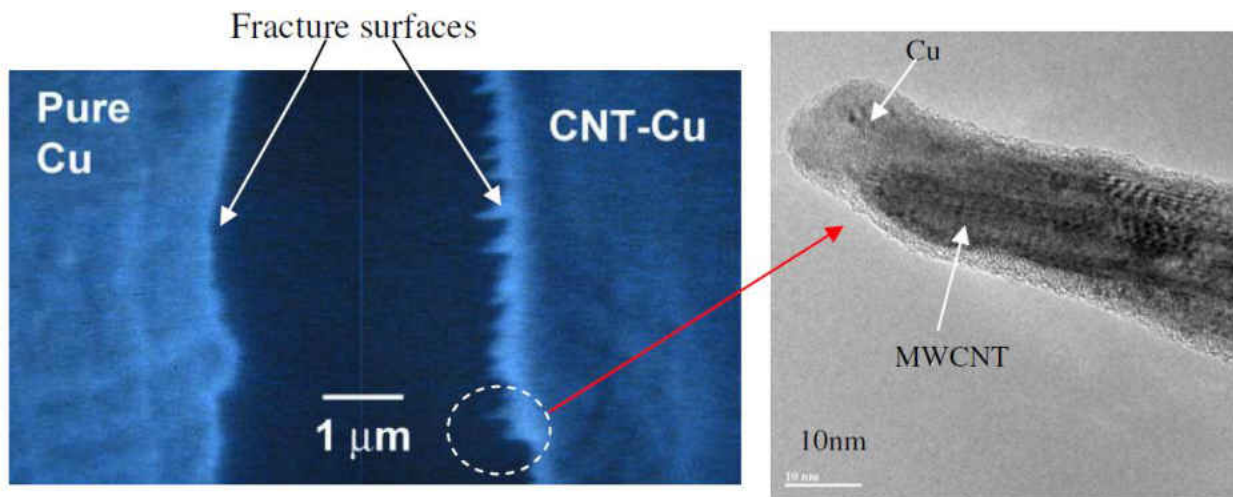
Figure 9 SEM fracture image of CNT reinforced copper and pure copper sample.
Indented fracture interface is showed in Cu/CNT nanocomposites, but it is smooth in pure copper. The enlarged TEM image on one tip in SEM shows the MWCNT is fully wetted by deformed copper. No broken up between CNTs and copper according to the TEM images[147].

Moreover, the ultimate tensile strength of CNTs reinforced copper is about 710 MPa, which is triple times greater than that of pure copper. But, the fracture strain of the Cu/CNT nanocomposite is much less than that of pure copper (Figure 8), but still produce enough ductility.

The fracture morphology of copper and Cu/CNT is scanned by SEM and TEM (Figure 9). It indicates that the fracture phenomenon of CNT reinforced copper is very different from pure copper. The fracture interface of Cu/CNT is indented curve which is different from pure copper's, which is quite smooth (Figure 9). When enlarging one tip of protrusion at fracture interface, TEM images show that the each individual CNT is fully enclosed by deformed copper (Figure 9), and there is no broken up take place between Cu and CNTs. This means that after deformation, there is no debonding at the interface between CNT and copper. This shows that there is high interfacial bonding force between Cu and CNT, which means a good interfacial bonding between Cu and CNT, is produced by electrochemical deposition process. The interfacial fracture bonding of electrochemical deposition is totally different from that of CNT/polymer composites and CNT/metal matrix composites which fabricated by power metallurgy which interfacial bonding is not good, and reinforcement is not large[11, 58, 59, 62, 147-149](<50%).
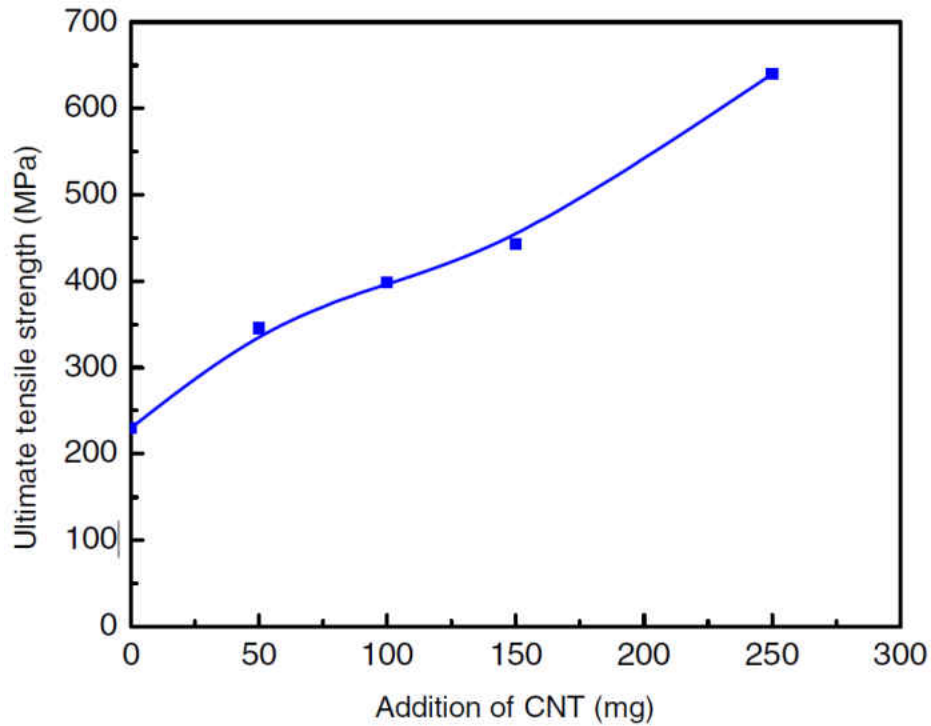
Figure 10 Tensile strength of Cu/CNT nanocomposite Vs CNT in copper electrolyte(mg L^{-1})[150]

A series test are conducted with various amounts of CNTs added to the composites to determine the influence of CNT in Cu/CNT nanocomposite, the result is showed in Figure 10. It shows that with the increase of MWCNT in the electrolyte, the tensile strength is increased in a polynomial pattern. This is because of the fact that more trapped MWCNT in the Cu/CNT composites result from more MWCNT added to the electrolyte.

3.3 Copper properties

Base on the experiment data, the first step is to determine pure copper properties which is a easy and direct process. True stress-strain curve is determined from engineering stress-strain which obtained from experiment data; yield stress and Young's modulus are determined from

true stress-strain curve. With these parameters, pure copper FEA model can be built up to predict its behavior.
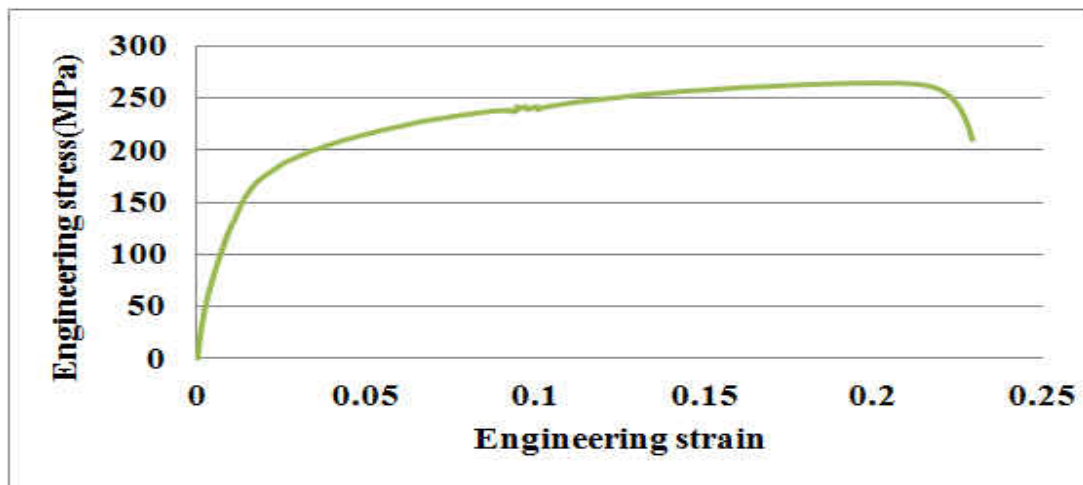
Figure 11 engineering stress strain curve of pure copper

In our thesis, σ_e and ε_e are denote engineering stress and strain, which are determined by the load and deflection with the model cross-section area A0 and length L_0 at t=0, σ_e and ε_e are determined as:

$$\sigma_e = \frac{P}{A_0} \quad \varepsilon_e = \frac{L}{L_0} \tag{1}$$

When strain is in low portion range in tensile experiment process, the behavior of many materials approximately obey Hooke's law, that is the stress is proportional to strain with a constant Young's modulus, which denoted by E:

$$\sigma_e = E \cdot \varepsilon_e \tag{2}$$

While as strain increases, many materials reach plastic deformation range, the point where material departs from linear relation is termed as yield stress. During plastic deformation, the nonlinearity associates with plastic flow in the parts, and microscopic structure and internal

21

molecular of materials undergoes a restructure procedure, the atoms moves to new equilibrium positions.

In LS-DYNA model, only true stress-strain rather than engineering stress-strain is accepted in the calculation, because materials' response in the plastic range can be measured more directly by true stress-strain curve. In this thesis, true stress strain cannot be obtained directly from experiment, only engineering stress strain relationship can be measured from experiment. Converting from engineering stress strain to real stress strain is a feasible way to obtain true stress strain relationship.

$$\sigma_t = P/A \qquad\qquad 3$$

$d\epsilon_t = \frac{dL}{l} \rightarrow \epsilon_t = \int_{L_0}^{L} \frac{1}{L} dL = ln\frac{L}{L_0} = ln\frac{A_0}{A}$ is termed as "true" or "logarithmic" strain.

The relationship between engineering stress and strain and true stress and strain can be written as:

$$\sigma_t = \sigma_e(1 + \epsilon_e) = \sigma_e\left(\frac{L}{L_0}\right) \qquad\qquad 4$$

$$\epsilon_t = \ln(1 + \epsilon_e) = \ln\left(\frac{L}{L_0}\right) \qquad\qquad 5$$

These equations showed above can be used to derive from engineering curve to true stress-strain relations before necking. Stress-strain relationship of ductile metals usually can be approximately described by simple power law relation form before necking:

$$\sigma_t = A\varepsilon_t^n \qquad\qquad 6$$

The parameter n is termed as strain hardening parameter, useful to determine the necking resistance. After necking, true stress strain relationship is determined through trail error procedure which is showed in Figure 13. Then the whole stress strain relationship of pure copper is determined which is showed in Figure 12; other copper parameters, Young's modulus and yield stress, also determined from this stress strain curve, density and poision ratio is obtained from other literatures[151], there parameters are showed in Table 1.

Table 1 Copper properties	
Density	8.94kg/m3
Young's Modulus	120GPa
Poision Ratio	0.34
Initial Yield stress	172MPa
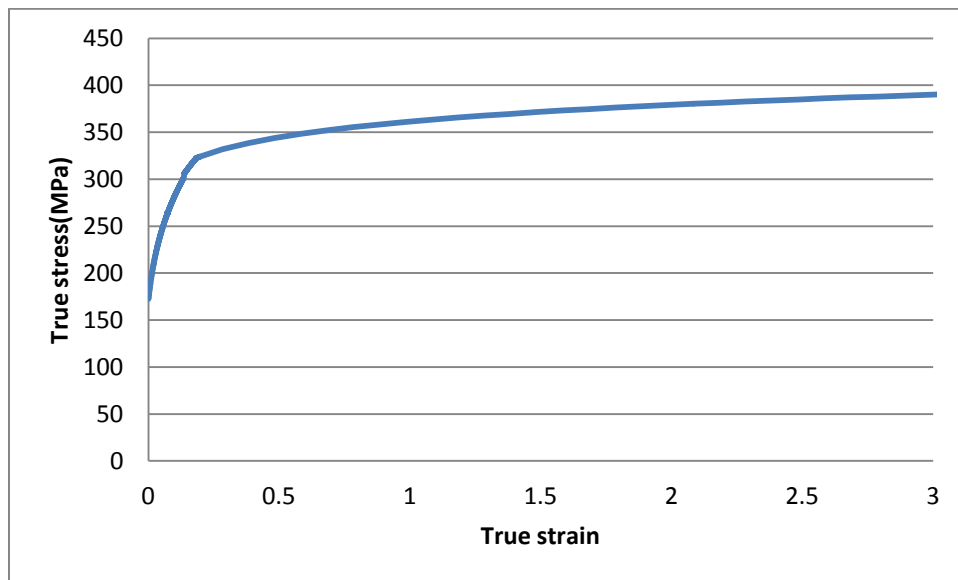
Figure 12 Pure copper fitted true stress strain curve

With this curve, we can calculate stress-strain relationship. Fitting the curve with experiment data, and employing the curve to represent stress-strain relation in our calculation, material deformation can be predicted.
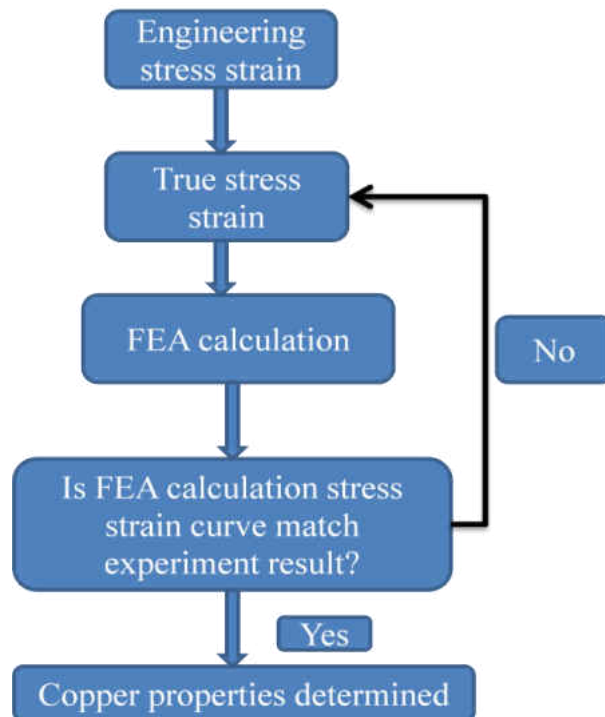
Figure 13 trial-error procedure
Trial-error procedure is employed to carry out several iterations, copper properties are determined after these processes, especially the stress-strain curve.
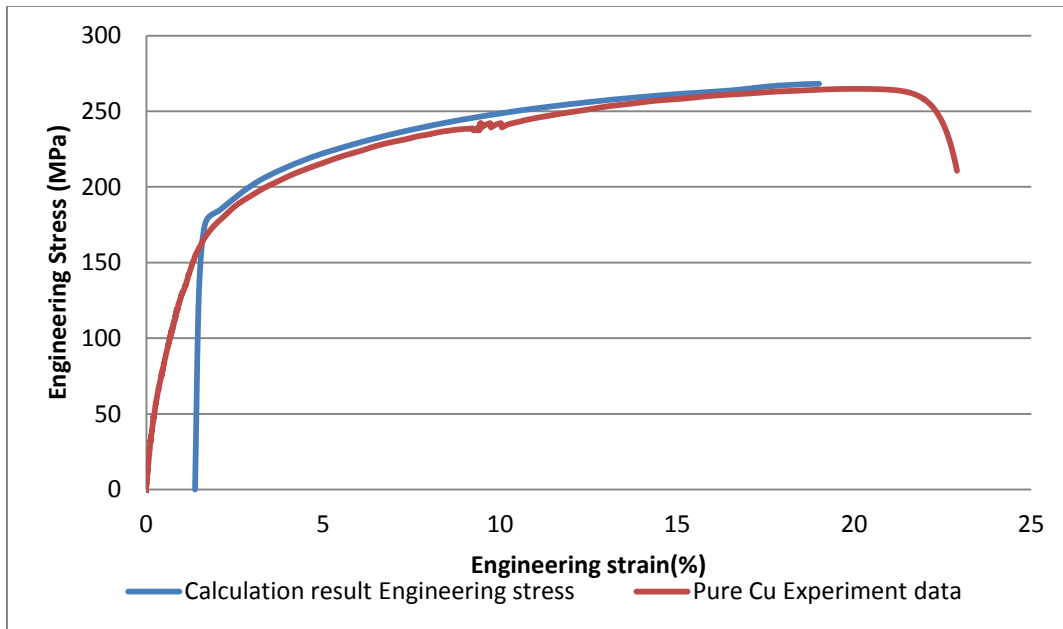
Figure 14 Engineering stress strain of pure copper calculation Vs Experiment

With copper properties and stress strain curve, copper behavior under tensile stress can be predicted. Pure copper model calculation result is showed in Figure 14, from the calculation result comparison showed, after imposing correct boundary conditions and proper material properties, calculation result fits experiment data well.

CHAPTER 4 NUMERICAL SIMULATION OF PURE COPPER

4.1 Finite element simulation

Finite element models are developed to predict Cu/CNT composite behavior and Ls-dyna is employed to simulate the deformation process. Figure 15 showed a simplified process to create models, simulate and analyze calculation results.
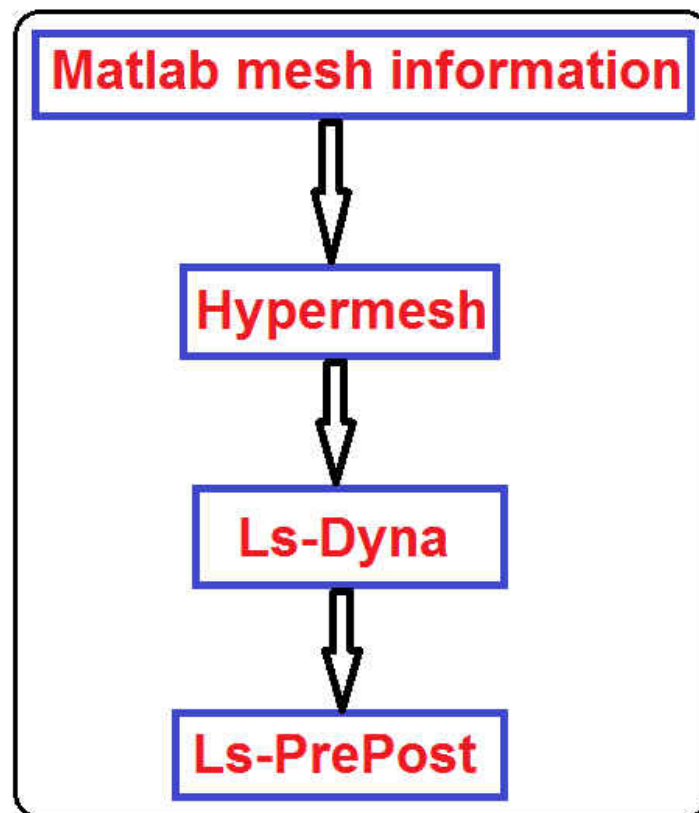
Figure 15 Simplified FEA process

In this process, the first step is to employ Matlab to generate FEA models files; these files include grid, element, load information and material information etc. Some common data is extract to one keyword file, which is called main keyword file; Ls-dyna includes these common

keyword files at the beginning of calculation automatically. The second step is to use hypermesh to open and review keyword files to see whether there is something wrong in the model or not. The third step is to open keyword to simulate and then analyze calculation result with Ls-PrePost.

To simplify the model and save calculation time, shell models are selected; shell model shape is showed Figure 16. The integration points through the thickness in our shell models are set to five, this is base on the balance of precise and efficiency of calculation. The meshing density near the location where fracture appear is set to very fine, and the density where is far away from the fracture is coarse.
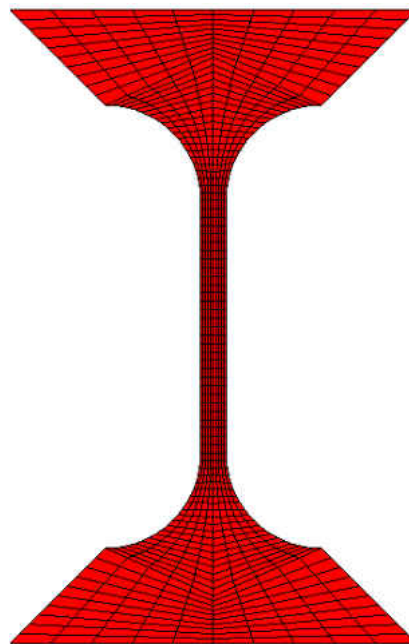
Figure 16 2D pure copper shell model

One approach which is widely used to deal with fracture in simulation is to delete elements or split elements where the criterion of fracture is achieved. However, these approaches are very sensitive to mesh size, because stain to fail increase with finer element meshes. Mesh size effect appear after strain localization, for ductile material this usually appear before initiation of fracture.

Localized deformation state is a state after an instable point, this state is termed as that all the deformations are concentrates in a small but finite area, this area is called necking region. Even external loading conditions do not change, the localized deformation occurs. As localization appears in this region, the structure outside localized region tend to unload elastically.
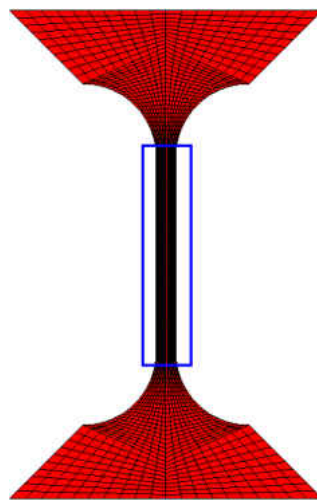
Figure 17 dog bone area to study mesh size

In this thesis, three different meshing are selected on the same specimen part to compare meshing size effect on model failure and fracture prediction, meshing information is showed in

Table 2. The number of elements in the Table 2 is the elements in the area which is circled Figure 17; this part is the area where necking and fracture takes place.

Table 2 Element size information

	Element size(nm)	Element number of boned gauge section
Mesh 1	40*33	1200
Mesh 2	20*22	3600
Mesh 3	10*11	14400
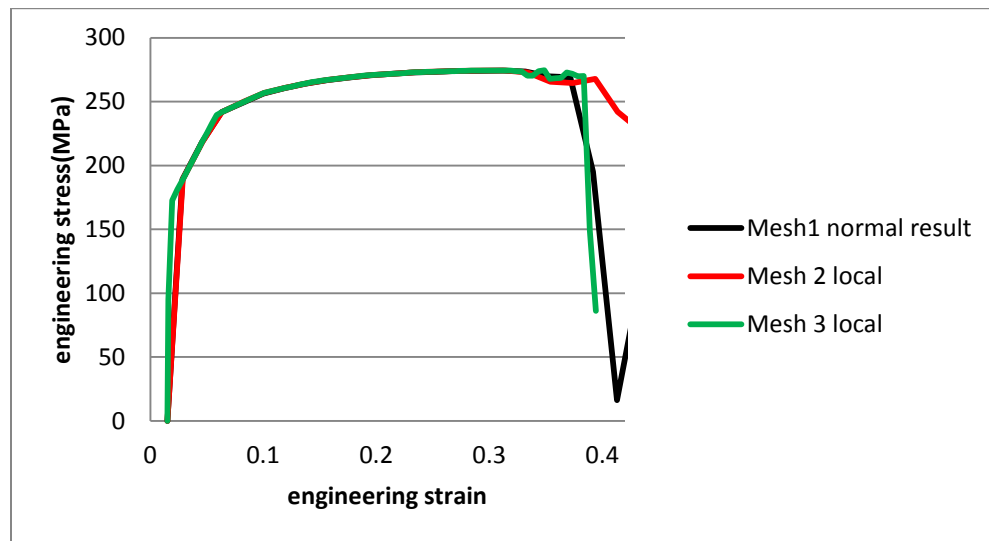
Figure 18 Stress-strain curve of three different meshing

In Figure 18, three calculations are conducted with three different element size; from the calculation result presented in Figure 18, we can see that different mesh size result to different failure and necking. But there is no difference before necking takes place. The mesh1 FEA simulation result is showed in Figure 19. At the beginning, the stress and strain fields are almost

uniform along the center of dog bone part, after localized necking stress and strain starts localize at the center of the part.
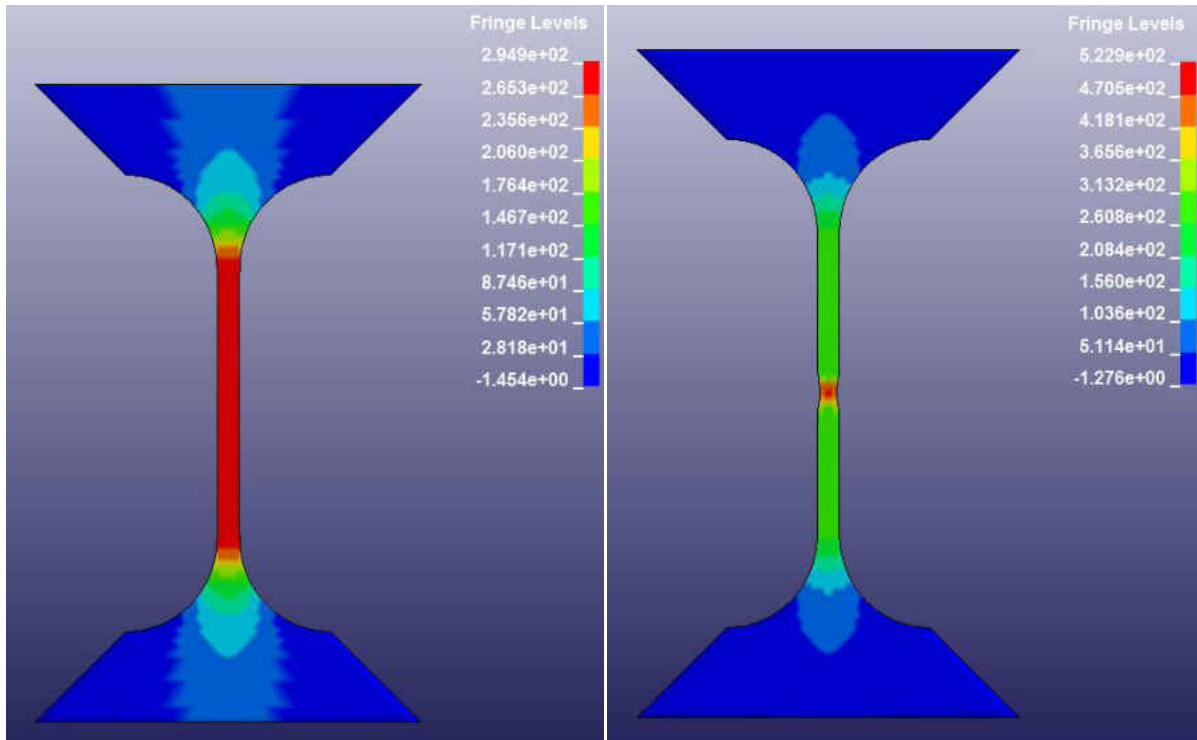
(a) FEA simulation before necking   (b) Simulation result after necking
Figure 19 Plastic strain contour plot of meshing 1

From the above discussion, we can conclude that the simulation result after necking is changing with meshing size. Then to predict plastic deformation after necking, one solution is to calibration mesh size; all the following FEA simulations should employ this mesh size to obtain same calculation result.

4.3 Nonlocal method in calculation

To solve the meshing size dependence, one feasible way is to employ nonlocal model in the plastic damage model. The nonlocal integral introduces long range micro structural

interaction by assuming the variable response at a material point is dependent on the state of its neighborhood in addition to the state of the point itself. The properties of one point are the average values within one radius, which is called characteristic length, the simplified theory is showed Figure 20.

In this research, we employ nonlocal method in Ls-dyna by adding key word "*MAT_NONLOCAL" in keyword file. The exponent of weighting function P is 8; the exponent of weighting function Q is 2; the characteristic length is 200nm to span a few elements in every model; the number of time steps between update of neighbors is 5.
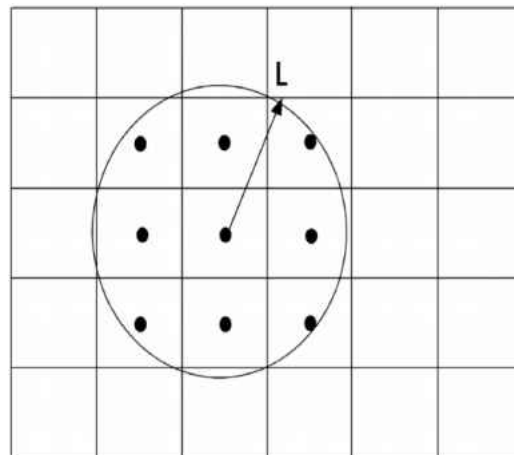
Figure 20 Material nonlocal mechanism
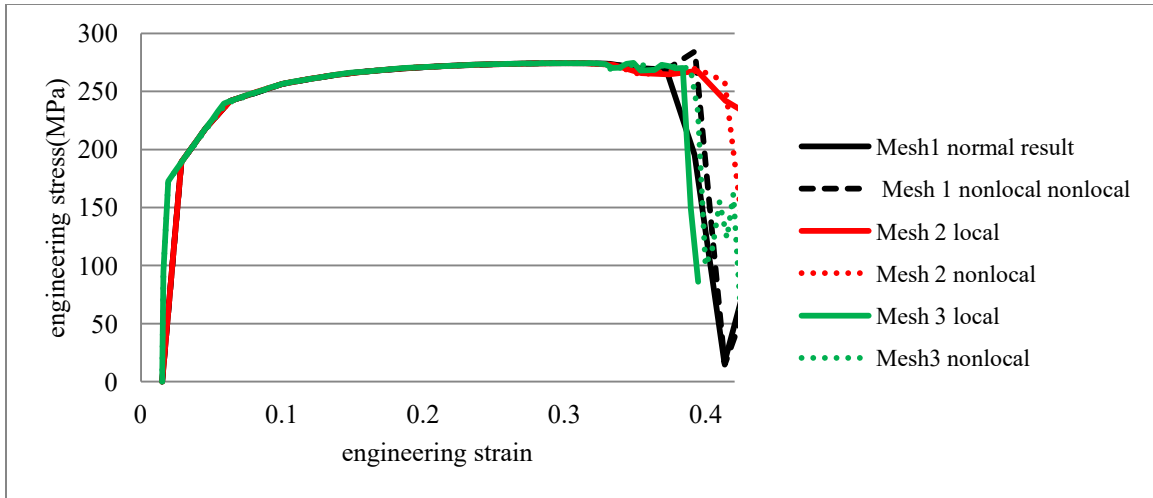
Figure 21 Calculation result with nonlocal method models

From the calculation that is showed in Figure 21, there is still big difference between three models after necking achieve in. In this calculation, we do not apply fracture criterion in the models, so all the model keep on necking in the calculation.

From the calculation that are showed above, we can conclude that many research claimed that nonlocal method can reduce meshing effect, our calculation result shows that nonlocal method cannot fully solve meshing effect on calculation.

4.4 Result discussion

In this chapter, we discussed ways to fit stress-strain curve in calculation in our models; base on the fitted stress-strain curve, we developed pure copper FEA models and employ nonlocal method to partially solve meshing effect during FEA calculation. The study shows that although many researches discussed on non-local method, our research shows that this method cannot fully solve mesh size effect on FEA simulation.

CHAPTER 5 NUMERICAL SIMULATION OF Cu/CNT COMPOSITES

5.1 Introduction

Residual stresses can be defined as those stresses that remain in a material or body after manufacture and processing without imposed of an external forces or thermal gradients[15]. Residual stress usually originates during manufacturing and processing of materials; the sources of residual stress are from heterogeneous plastic deformation (mechanically generated), thermal contractions (thermally generated) and phase transformations (chemically generated)[15]. In our research, chemically generated residual stress is mainly considered in our research, because Cu/CNT composites produced by electrochemical de-position process. Due to volume changes result from electrochemical reaction and phase changes in Cu/CNT composite manufacture process, residual stress is generated between CNT and copper matrix, in composite material, the copper with residual stress is called hardened region. Harden region and its volume fraction plays key roles in changing composites hardness, which is discussed in this chapter.

In our research, we employ implicit algorithm of LS-DYNA. To determine required time step in explicit algorithm, LS-DYNA goes through all the elements. To make calculation stable, time step is decreased by a scale factor of 0.9(default):

$$\Delta t = 0.9 \frac{l}{c}$$

$$c = \sqrt{\frac{E}{\rho}}$$

l:length of an element   E:material Young's modulus

Time step decrease about 1×10^9 times because of elements nano-scale length. But in the LS-DYNA implicit, time step has nothing to do with element size, so we choose implicit algorithm in this thesis.

Table 3 is the list of parameters which are studied in this thesis.

Table 3 Parameter in study

Parameters	Parameters meaning
σ_y	composite material yield stress
σ_0	pure copper yield stress
H	Composite model length
D	Composite model diameter
f_v	CNT volume fraction in composite model
f_H	Hardened region volume fraction
Harden strain	residual strain of the copper around CNT

5.2 2D Unit cell model prediction for elasticity, initial yield and strain hardening

Deformation and failure of Cu/CNT composite is studied numerically in this chapter. In our calculation, we construct a 2D unit cell FE model which consists of both metal matrix and CNTs. A model picture is showed in Figure 22, CNT volume fraction of this unit cell model is 2%; the red area represents CNTs, and the blue area represents the pure copper with residual strain which come from the affection CNTs during composites manufacture. The yellow area represents the copper which is not affected by CNTs during composite manufacture. The aspect ratio of three parts is choosen to be the same in our models. To simplify the model and save

calculation time, we employ symmetry method on our models. Only one-fourth of specimen is selected in calculation, symmetry boundary is employed on y=0 and x=0.
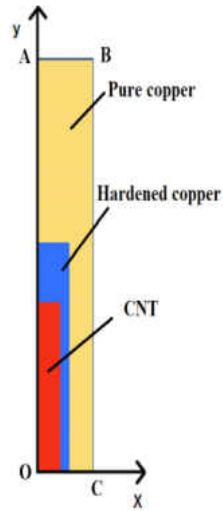
Figure 22 Simplified unit cell models

Different colors on the picture represent different materials in the models. Yellow part represent pure copper; blue region represents hardened copper; red region represent CNTs.

Table 4 Unit Cell Boundary conditions(B.C.)

OA	X symmetry B.C.
AB	Velocity B.C.
BC	global linear B.C.
OC	Y symmetry B.C.

The radius of pure copper, harden area and CNT are denoted by R_{cu}, R_H and R_{CNT}, the length of three areas are H_{cu}, H_H and H_{CNT}.

The boundary conditions for the cell region analyzed numerically are showed in

Table 4:

At x=0, the symmetry boundary is automatically applied in calculation because we employ "Axisymmetric solid (y-axis of symmetry)" as element formulation in our calculation.

The boundary conditions(B.C.) for the 2D unit cell model are:

$u_y=0$ on y=0

$u_y=U2$ on y=H/2

$u_x=U1$ on x=Rcu

In ls-dyna the keyword "CONSTRAINED_LINEAR_GLOBAL" is applied to the models to fullfill cell region boundary conditions above. In the models, with this constrained boundary, the composite materials is reinforced greatly, the details of keywords is showed in Table 5.

Table 5 constrained Linear boundary conditions

*CONSTRAINED_LINEAR_GLOBAL		
NID	DOF	COEF
1	1	-1

5.3 Effect of aspect ratio, CNTs volume fraction, Harden strain and its volume fraction to the model

In unit cell models, previous studies[9] show that different aspect ratios of CNT and copper area are key parameters that affect calculation results greatly. In our research, we did a series of simulation on different aspect ratios to find out the relationship of material hardening

with other parameters. To simplify the model, we suppose that the deformation CNT is still in elastic deformation range.

Before study CNT metal matrix composite materials characteristic, the mechanic properties of CNT are important. Base on the previous studies, there are different way to study mechanics properties of CNT, K.M.Liew etc[11, 12] employed molecular dynamics simulation to determine CNT properties by means of investigating molecular reaction. This method consider both elastic and plastic behavior. Xiao etc[10] employed a simplify molecular structural mechanics model, which suppose there is only Morse potential interatomic reaction, which only produce elastic strength. Many experiments[28, 29] were also developed test plasticity and elasticity of CNT. From molecular dynamics simulation[11], the aspect ratio CNTs in the composites can also change composites hardening greatly. Reference [12, 152] states that the elastic properties of CNT are nearly independent of the indices but not for the plastic deformation. With the same radius, the elastic limits of Zigzag (n,0) CNTs are nearly twice that of Armchair (n,n) CNTs [12, 152].

Based on the molecular calculation [12], the stress strain curve follows as follow. At $0 \leq \varepsilon \leq \varepsilon_p$, the stress-strain relationship follows the Hooke's law, i.e. $\sigma = E\varepsilon$, where ε_p is the proportional strain limit point. As the strain increases, the stress-strain behave non-linearly until it reaches the yield strain ε_s. The stress-strain curve is represented as $\sigma = (A\varepsilon + B)\varepsilon$ at $\varepsilon_p \leq \varepsilon \leq \varepsilon_s$. A and B are determined by curve fitting from MD calculation, which is showed in Table 7, where computation result and fitted curved parameters are listed. After yield point, large plastic deformation without an obvious stress increase; before yield stress $\varepsilon_s \leq \varepsilon \leq \varepsilon_h$, the stress can be

approximately as σ= σ_s; from dσ/dε=0, σ_s=-B/(2A). We choose mechanics parameters of two-walled CNT with L/D=9.1 in our following composite model.
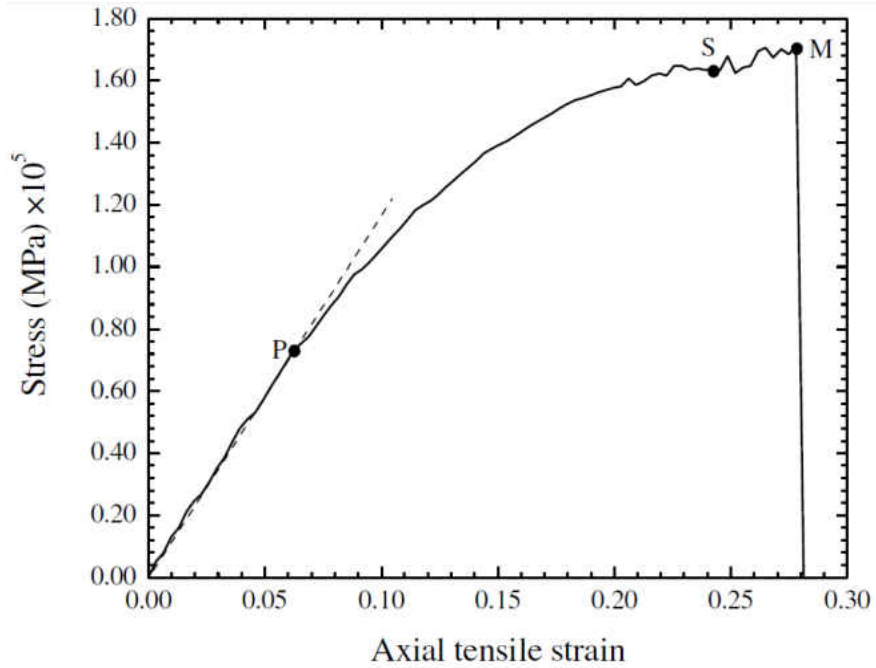
Figure 23 engineering strain stress curve of CNT molecular dynamics calculation result[12]

Table 6 CNT properties[12]

Young's Modulus(TPa)	1.175
Yield strength (GPa)	163.3
Tensil strength(GPa)	168.4
Proportional strain limit(P point)	0.0621
Elastic strain limit(S point)	0.242
Max strain(M point)	0.281
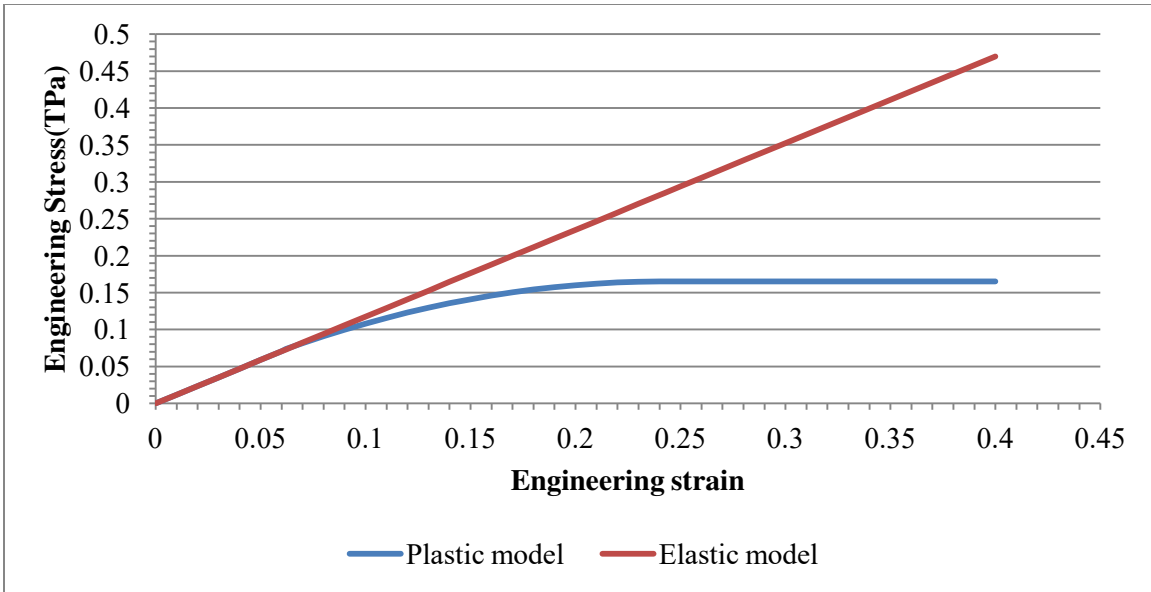
Figure 24 smoothed and fitted stress-strain curve from CNT MD(molecule dynamic) calculation.

Table 7 Material properties of selected single and multi-walled CNTs[12]

	L/D	Young's modulus (Tpa)	A (TPa)	B (TPa)	proportional strength(Mpa)	Yield strength (Mpa)	Tensile strength (Mpa)	Proportional strain limit	Elastic strain limit	Maximum strain
Single-walledCNT of (10,10)	4.5	1.043	-2.625	1.211	6.103×10^4	1.369×10^5	1.404×10^5	0.0585	0.231	0.280
	9.1	1.031	-2.522	1.190	6.271×10^4	1.421×10^5	1.485×10^5	0.0594	0.236	0.279
Two-walled CNT of (5,5) and (10,10)	4.5	1.161	-2.543	1.259	7.231×10^4	1.614×10^5	1.624×10^5	0.0627	0.247	0.279
	9.1	1.175	-2.810	1.362	7.287×10^4	1.633×10^5	1.684×10^5	0.0621	0.242	0.281
Three-walled CNT of (5,5), (10,10) and (15,15)	4.5	1.000	-2.358	1.160	6.068×10^4	1.430×10^5	1.434×10^5	0.0605	0.238	0.281
	9.1	0.972	-2.275	1.120	5.645×10^4	1.381×10^5	1.414×10^5	0.0611	0.246	0.282
Four-walled CNT of (5,5), (10,10), (15,15) and (20,20)	4.5	0.932	-2.234	1.103	6.075×10^4	1.343×10^5	1.382×10^5	0.0654	0.235	0.281
	9.1	0.872	-2.132	1.023	5.784×10^4	1.278×10^5	1.327×10^5	0.0633	0.241	0.280

<u>5.4 Parametric study tool kits</u>

To study the different parameters effect on composite models in our project, we need to build up large amount of keyword files for Ls-dyna, and batch files to call Ls-dyna to launch keyword files one by one automatically. These parameters include elements size, specimen dimensions, specimen aspect ratio, CNT volume fraction, harden copper volume fraction, copper volume fraction, and residual strain of harden copper. All the keyword files are created based on these pre-determined parameters.

Tool kits for Post-processing the simulation results are also developed, to increase the efficiency of data processing.

5.4.1 Input deck generator

To find out parameters, such as aspect ratio, volume fraction, effect on composite models, a series of keyword files created with a series of parameters. In our studies, different function of keywords files are separated into different keyword files, main keyword files is "CuCNT_model.k" which includes every other keyword files and provides common control information; meshing information is in "mesh.k"; material information is packed in "material.k" files; special boundary conditions are packed in "BC_Right.k" and other files.

All the meshing information is created by our tool kits; the array of the node is formatted as showed in Figure 25(a), element numbering structure is similar to node numbering structure, the node number is increase from left to right, from bottom to top. Volume fraction separation points are the points which separate two materials; these points are showed in Figure 25(b). Volume fraction is calculated base on meshed node, the nodes which are the nearest to the

volume fraction separation point is selected as the border of two materials. To generate a series keyword files, we need simply redo the procedure mentioned above.
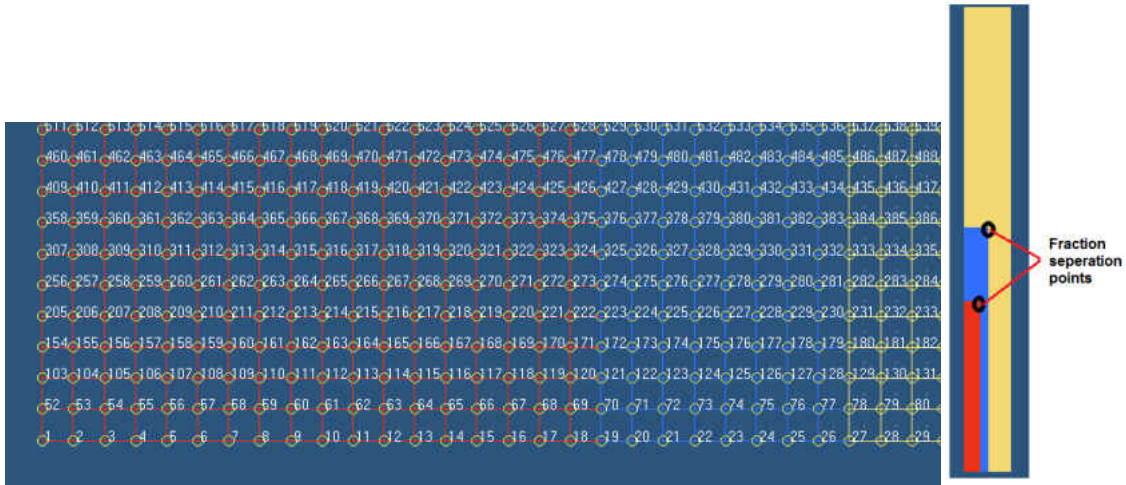
Figure 25 Meshing node array format
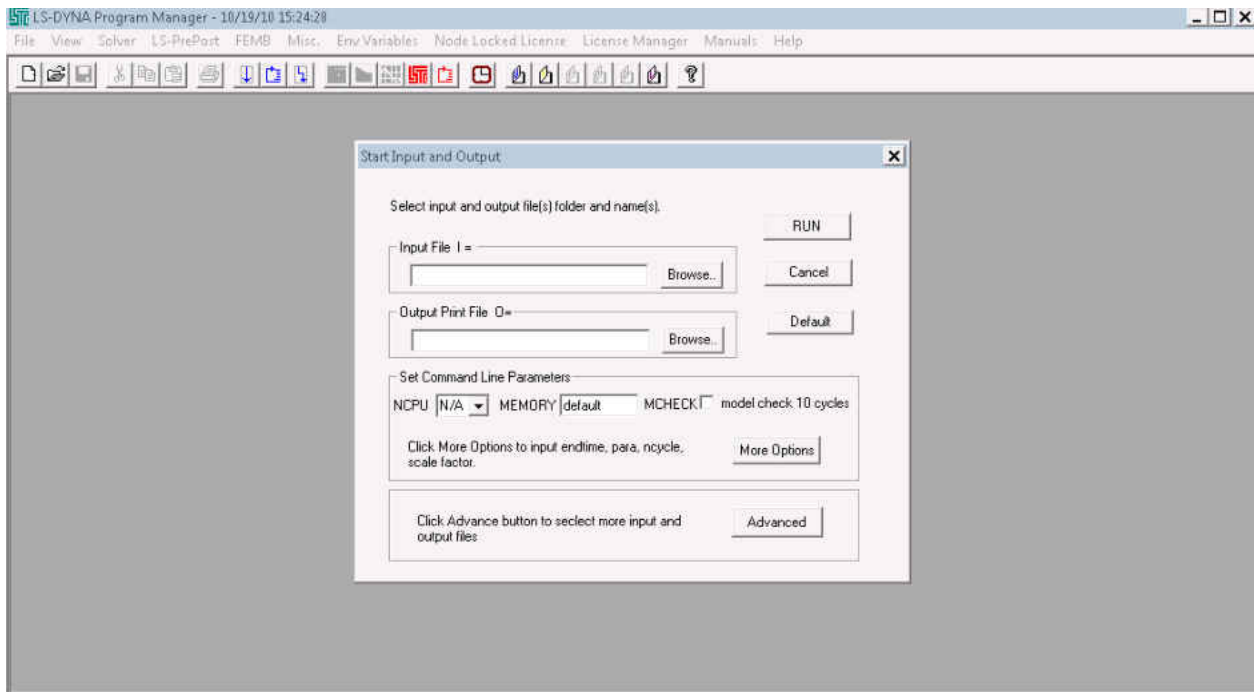
Figure 26 Ls-Dyna launch keyword dialog

Although Ls-Dyna provides interface dialog to user to launch keyword as showed in Figure 26, its efficiency is low when large amount of jobs to import into Ls-Dyna. In our research, we employ batch files to launch keyword files and Ls-Dyna solver directly with command line. A main batch file launches each sub-batch file one by one automatically; the routine of this process is showed in Figure 27.

```
        ┌──────────────────────┐
        │   Main batch files   │
        └──────────────────────┘
                   ▲
    ┌──────────────┴──────────────────────────┐
┌──────────────────────┐            ┌──────────────────────┐
│   ┌──────────────┐   │            │   ┌──────────────┐   │
│   │Sub-batch file│   │  . . . . . │   │Sub-batch file│   │
│   └──────────────┘   │            │   └──────────────┘   │
│          ▲           │            │          ▲           │
│   ┌──────┴──────┐    │            │   ┌──────┴──────┐    │
│┌──────────┐┌─────────┐            │┌──────────┐┌─────────┐
││Keyword file││Ls-Dyan Solver│     ││Keyword file││Ls-Dyan Solver│
│└──────────┘└─────────┘            │└──────────┘└─────────┘
└──────────────────────┘            └──────────────────────┘
```
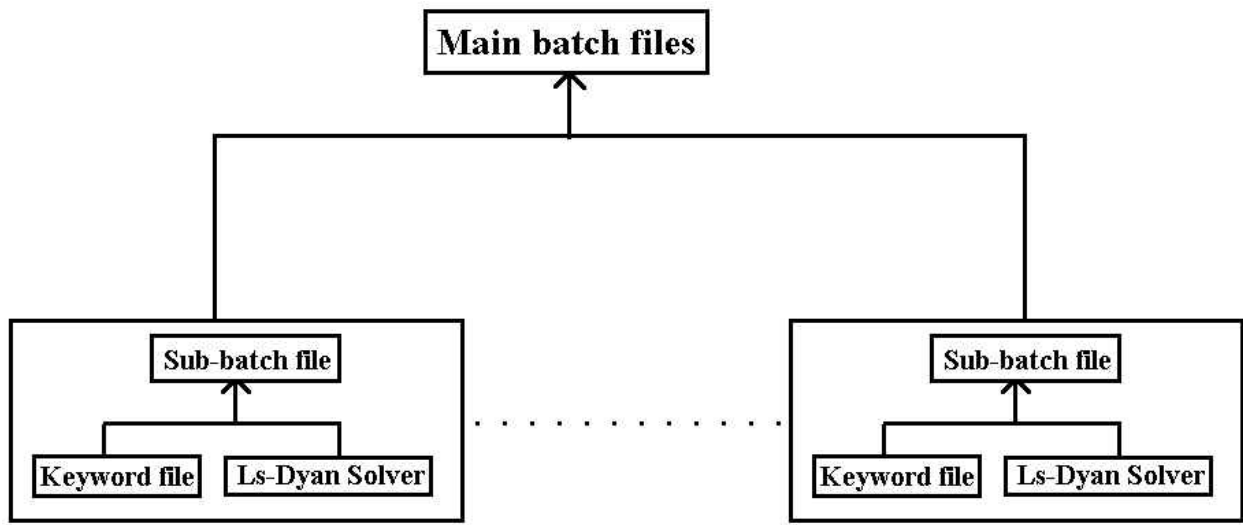
Figure 27 Keyword and Ls-Dyna solver launches procedure by batch files automatically

5.4.2 Ls-Dyna post-processing code

Ls-PrePost is the software developed by Ls-Dyna to post-process Ls-Dyna calculation result. But its efficiency is also low to deal with large amount of results. Node displacement and total force in y-direction of selected nodes are all exported to specific files which are parsed by our tool kits. After parsing the outputted data, results and experiments are all plotted at the same picture, which provide very fast and convenient way to see and compare result.

5.5 Calculation result

5.5.1 Different CNT volume fraction and model aspect ratio

To study different factors in calculation, we did a series of calculation based on CNT volume fraction and model aspect ratio. In our model, we apply same aspect ratio on three different areas. X-axis is the CNT volume fraction, Y-axis is the H/D ratio, Z-axis is normalized composite yield stress to pure copper yield stress. The first step is to consider all the deformation of CNT as elasticity only. The Young's modulus is 1.175TPa.

"H/D" represents the aspect ratio of model, all the areas in our model are the same aspect ratio, which include CNT, hardened area and pure copper.

"fv" represent the volume fraction of CNT in the composite material, also to better understanding, we also convert the volume fraction to mass fraction with equation for Cu/CNT composites

$$f_m = \frac{f_v * 2.1}{2.1 * f_v + (1 - f_v) * 8.94}$$

The density of carbon nanotube is 2.1g/cm^3[153], the density of pure copper is 8.94g/cm^3, relationship lists volume fraction and mass fraction of CNT relationship in

Table 8.

"σ_y/σ_0" represent the yield stress of composite material to yield stress of pure copper

The harden strain is 0.5. The volume fraction of hardened area is 0.1. H/D ratio is range from 0.1 to 100, CNT volume fraction is range from 1% to 7%.

Table 8 fraction ratio in our model

Volume fraction	Mass fraction
0	0
0.01	0.002367104
0.02	0.004770992
0.03	0.007212529
0.04	0.009692606
0.05	0.012212142
0.06	0.014772088
0.07	0.017373422
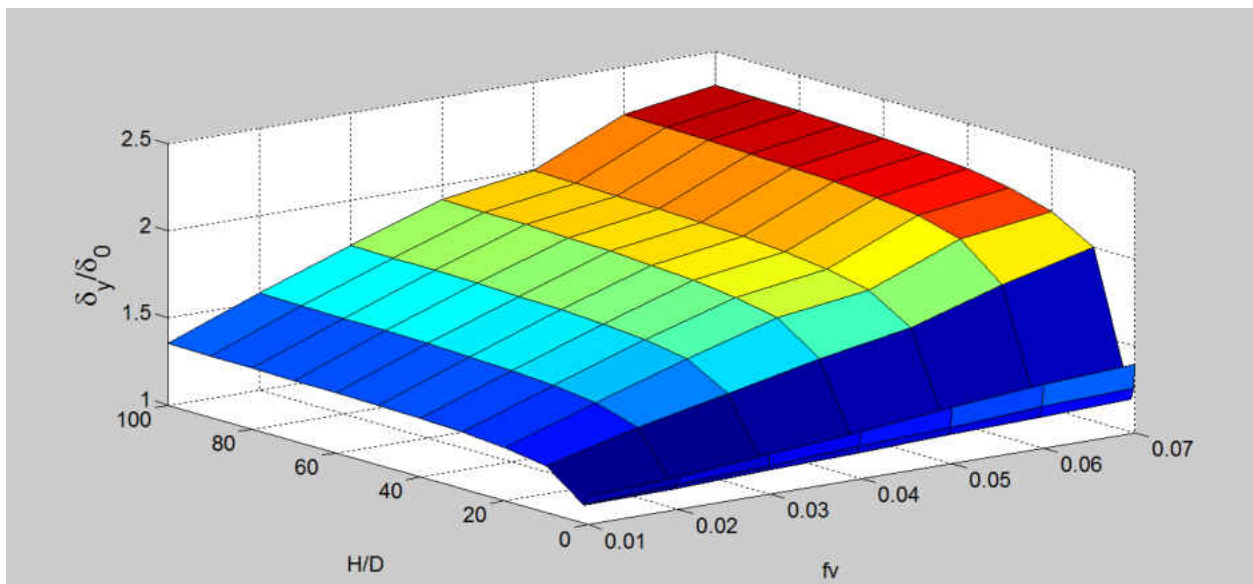
Figure 28 CNT elastic model with different copper aspect ratio and CNT volume fraction

From the calculation result showed in Figure 28, we can see that the fv increases, the yield stress increases monotonically; but to the aspect ratio (H/D), for the same fv, σ_y/σ_0 reaches its minimum values at H/D=1; but aspect ratio (H/D) effects decrease significantly after H/D≈10. Also as the increase of H/D, the effect of fv increases at the same time.
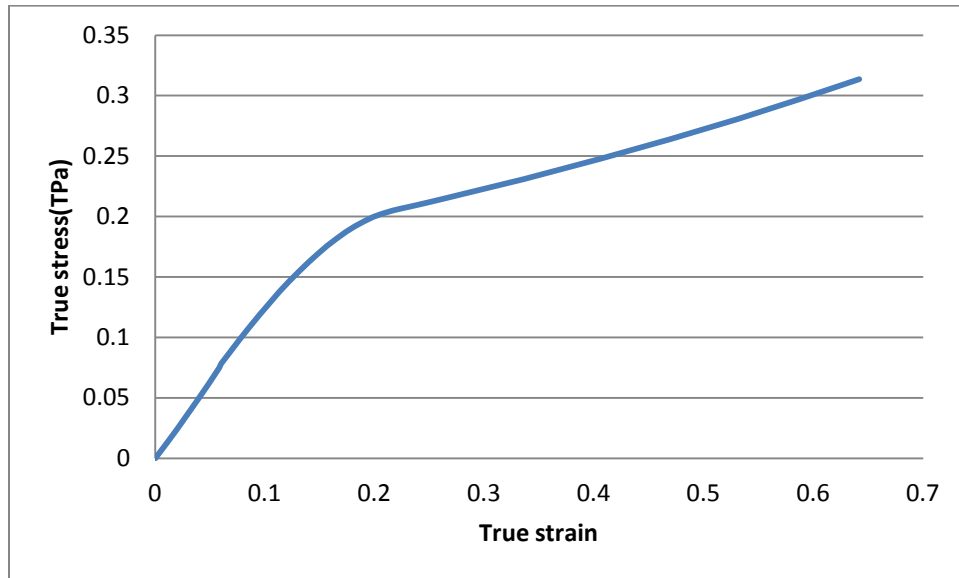
Figure 29 True stress strain of CNT with plastic properties
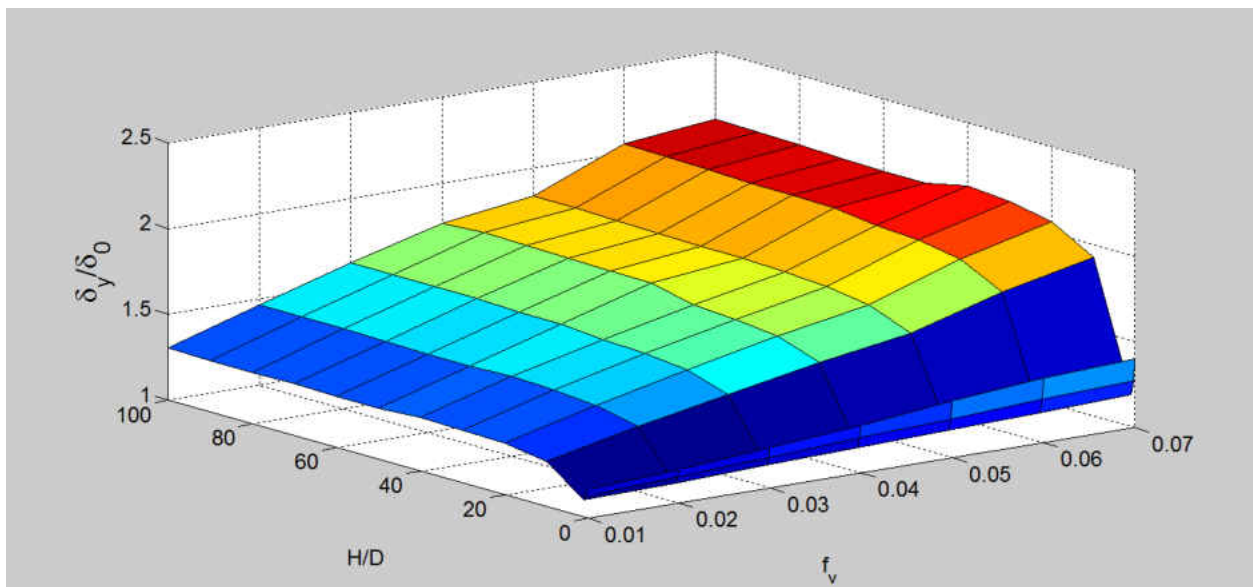
Figure 30 CNT plastic model with different copper aspect ratio and CNT volume fraction

Our next step is to study the plasticity of CNT effect on the composite materials. The engineering stress-strain relationship is obtained from Table 7, and is converted to true stress-

strain relationship by the process which is presented in chapter 3.3; true stress-strain curve is plotted on Figure 29.

Figure 30 indicates that in comparison with the model with only elastic properties, the yield stress of elastic-plastic CNT decrease significantly. This means that hardness of composite decreases because of CNT plasticity.
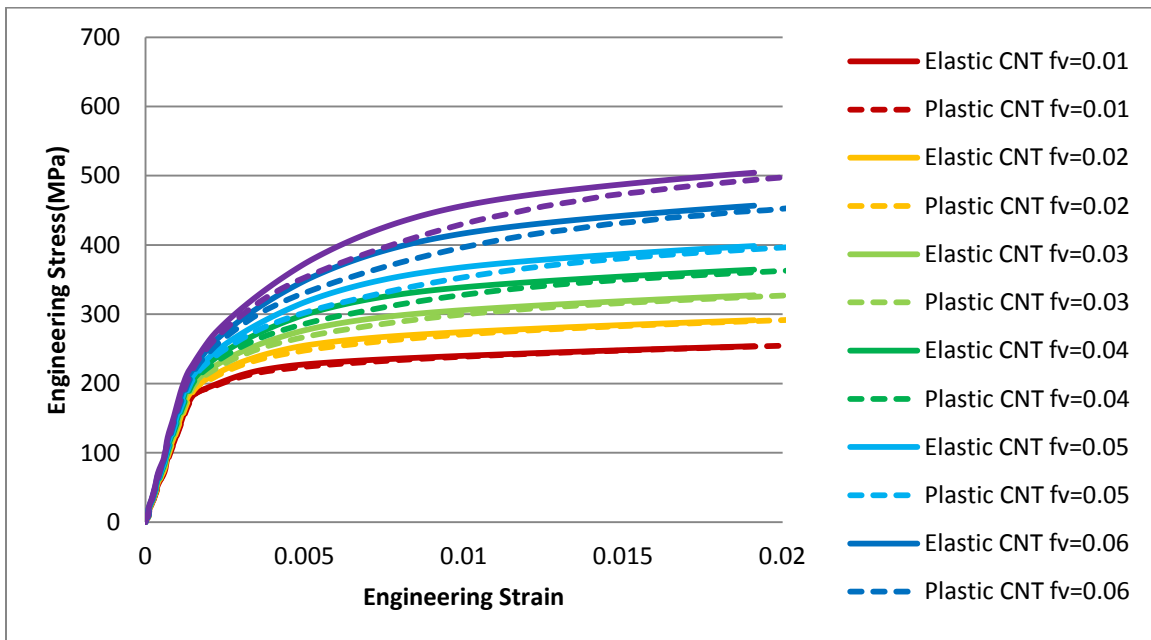
Figure 31 Volume fraction trend

To better evaluate CNT volume fraction roles in models, a series of calculation results are plotted together in Figure 31. Model results with elastic CNTs and elastic-plastic CNTs are plotted at the same time, for the same CNT volume fraction. Models with elastic CNT is always stiffer than the one with plastic CNT. With the increasing of CNT volume fraction, the composites becomes harder and harder. It is found that CNT plasticity plays much less roles in reinforcing copper.

5.5.2 Harden volume fraction and harden strain effect on composite material

Previous studies show that there is a transition area between CNT and pure copper, this area plays import roles in changing composite materials properties. We constructed a series models to study the effect of harden strain and harden copper volume fraction. In this model, we suppose that all the CNT deformation is in elastic deformation range, no plastic deformation is considered. The X-axis is the volume fraction of hardened copper; Y-axis is the different harden strain of copper; Z-axis is the normalized yield stress of composites by that of pure copper.

A series calculation results are combined and showed in Figure 32. From the Figure 32 we can see that with the increase of harden strain and volume fraction, the yield stress of composite increases monotonically with harden strain and volume fraction of harden area.
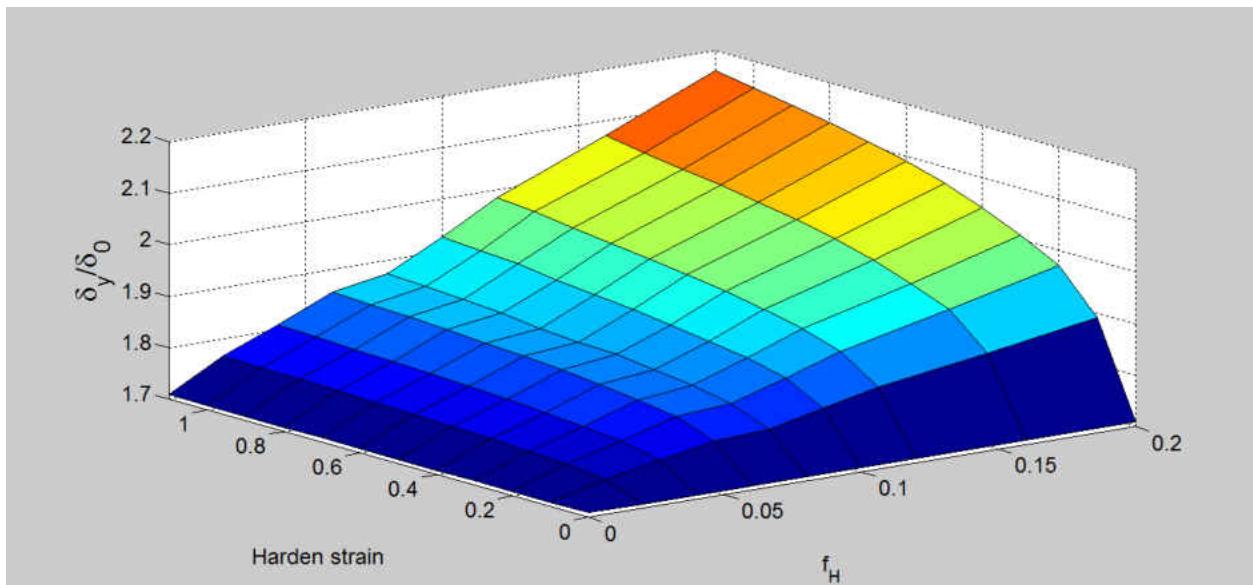
Figure 32 CNT elastic model with different copper harden strain and different the copper harden volume fraction
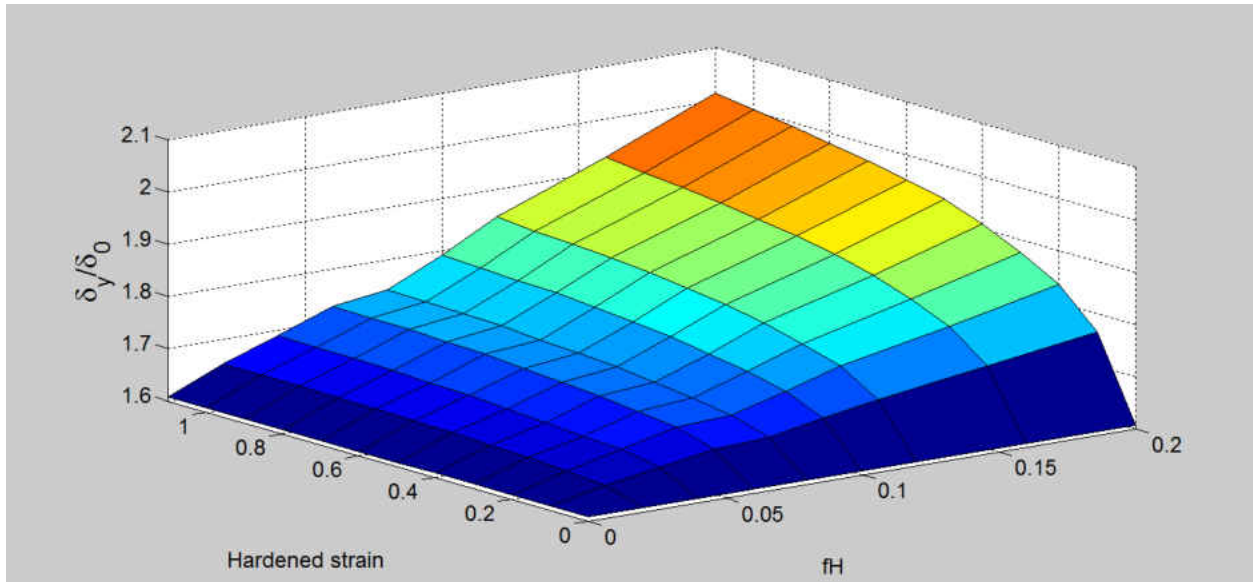
Figure 33 CNT plastic model with different copper harden strain and different the copper harden volume fraction

On the other hand, to evaluate the effect difference between elastic model and plastic model, plastic deformation of CNT is considered in the model. Same series of calculations are conducted, the only difference between elastic model and plastic model is the CNT stress-strain curve. For the model considering plasticity, stress strain relationship is not simply follow Hooke's law.

5.6 Correlation between experiments and simulations

Based on the parameters study in the previous chapter, we can find that there are many parameters in the models that can affect composite hardness. To fit the calculation result with the experiment result, suitable mechanic properties should picked up from the series calculation. It should be noted that the mechanics parameters which are picked from different is not the only

choice, because change different parameters can have the same effect on the composite. Good

correlation was achieve for a set of carefully choose parameters, as shown in Figure 34.
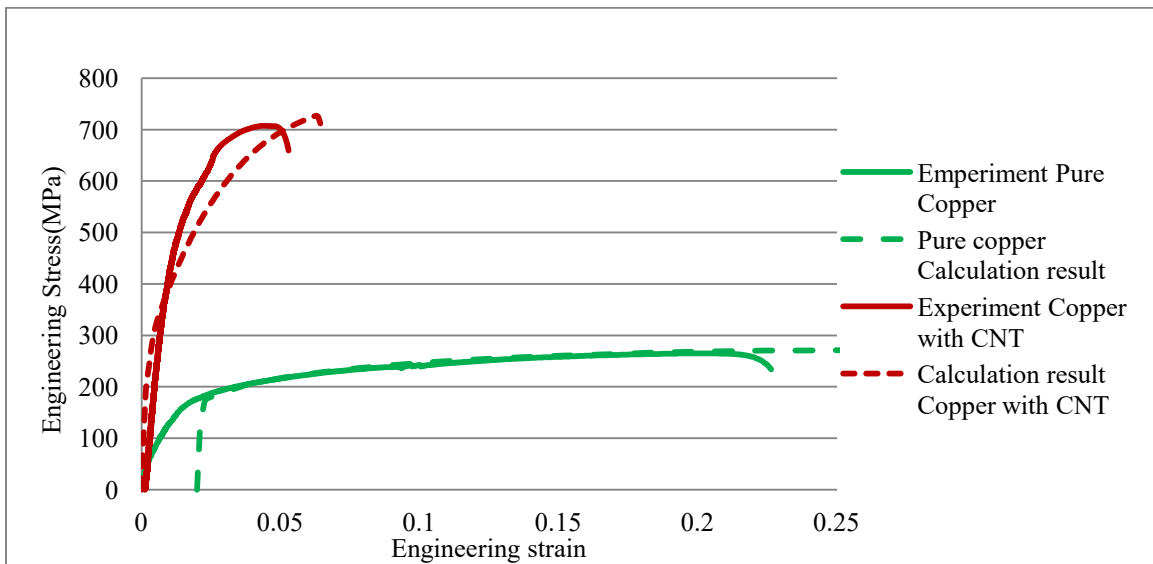
Figure 34 Calculation result of correlated parameters

5.7 Result discussion

In this chapter, we developed unit cell models and a series of tool kits to study mechanic

properties of CNT composites. Unit cell modeling is a simplified way to calculate composite

material properties. By imposing proper boundary conditions, geometry factors and volume

fraction of different area inside composites, the model can predict correct hardness of the

composite. Our calculation result can fit experiment result.

It is found that CNT in composites material cannot reinforce the material to the expect

hardness, there must some other factors that play important roles to reinforce the materials. What

we assume is that there is a hardened area around CNT in the composite materials, which plays important roles in reinforcing composites material hardness.

The aspect ratio of a model is another factor which can change composite models hardness dramatically. In our model, the aspect ratio of three area are all the same. At the aspect ratio of H/D=1, the effect of CNT reach its minimum level. The composite material hardness increases monotonically as H/D>1 or H/D<1. This trend is showed in Figure 28 and Figure 30. While our research only focus on H/D>1; the reinforcement of CNT has only slight difference after H/D≈10, so in our calculation, the MD calculation result of H/D=9.1which is showed in Table 7 is used as our uniform CNT properties.

We also found that the residual strain around CNT also plays important roles in reinforcing composite materials. The hardness of composite material increases monotonically with both harden strain and its volume fraction.

CHAPTER 6 PRELIMINARY RESULT ON 3D UNIT CELL MODEL

2D unit cell model is a simplified model, because all the materials in composite are simplified to be a uniform region. In the actual conditions, CNT disperse in the composites randomly, but our 2D unit cell models suppose that CNT is uniformly distribute among metal matrix. A 3D unit cell model is built in this chapter to get preliminary result.

6.1 3D Cu/CNT composite model dimension & geometry

3D unit cell model is a more precise model. In our research, we build up 3D geometry with ProE, both position and directions of CNT are randomly dispersed inside composites. To simplify model and save computer time, symmetry boundaries are also imposed on the model, one-eighth of the whole model is selected. The one-eighth length of model is 250nm, cross-section of model is square, and one-eighth width of CNT model is 100nm. One-eighth model geometry shape is presented in Figure 35, the surface number and boundary on each surface is showed in

Table 9. The CNTs dimension in the 3D models are 10nm(Diameter)×50nm(Length).

Table 9 3D model surface information

surface	surface number	boundary condition
left	1	fixed at 1,5,6
bottom	5	fixed at 3,4,5
back	4	fixed at 2,4,6
right	2	fixed at 5,6 and global linear equation at 1
front	3	fixed at 4,6 and global linear equation at 2
top	6	velocity boundary
		note: the number in this column represent degree of freedom
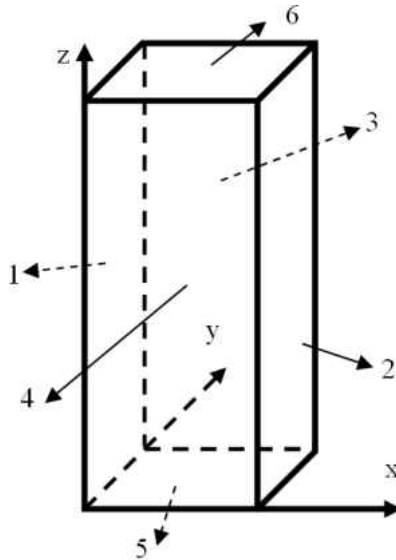
Figure 35 3D unit cell model with proper boundary conditions

6.2 3D Cu/CNT composite model meshing

Because the volume inside composite model is irregular, we have to employ tetra mesh function in Hypermesh to create tetrahedron elements, which can fill any 3D volume space. The first step is to generate surface shell mesh. Most of the surfaces meshing elements are quads. Initially 3D volume meshing elements are created based on the surface meshed elements. The mesh density of CNT surface mesh elements are much smaller than the surface mesh near model surface, because strain/stress gradient at CNT and metal matrix interface is much larger than other places.

A meshed model is showed in Figure 36 , model Figure 36(a) is viewed from XZ plane, Figure 36(b) is the cross-section of the model which is viewed from XY plane. The red region of the model is pure copper, and the blue region is CNTs. The mesh density around CNTs is much higher than other region, because more attention is focused on the interaction between CNTs and copper matrix. The total number of elements of this model is one million.

(a)   (b)
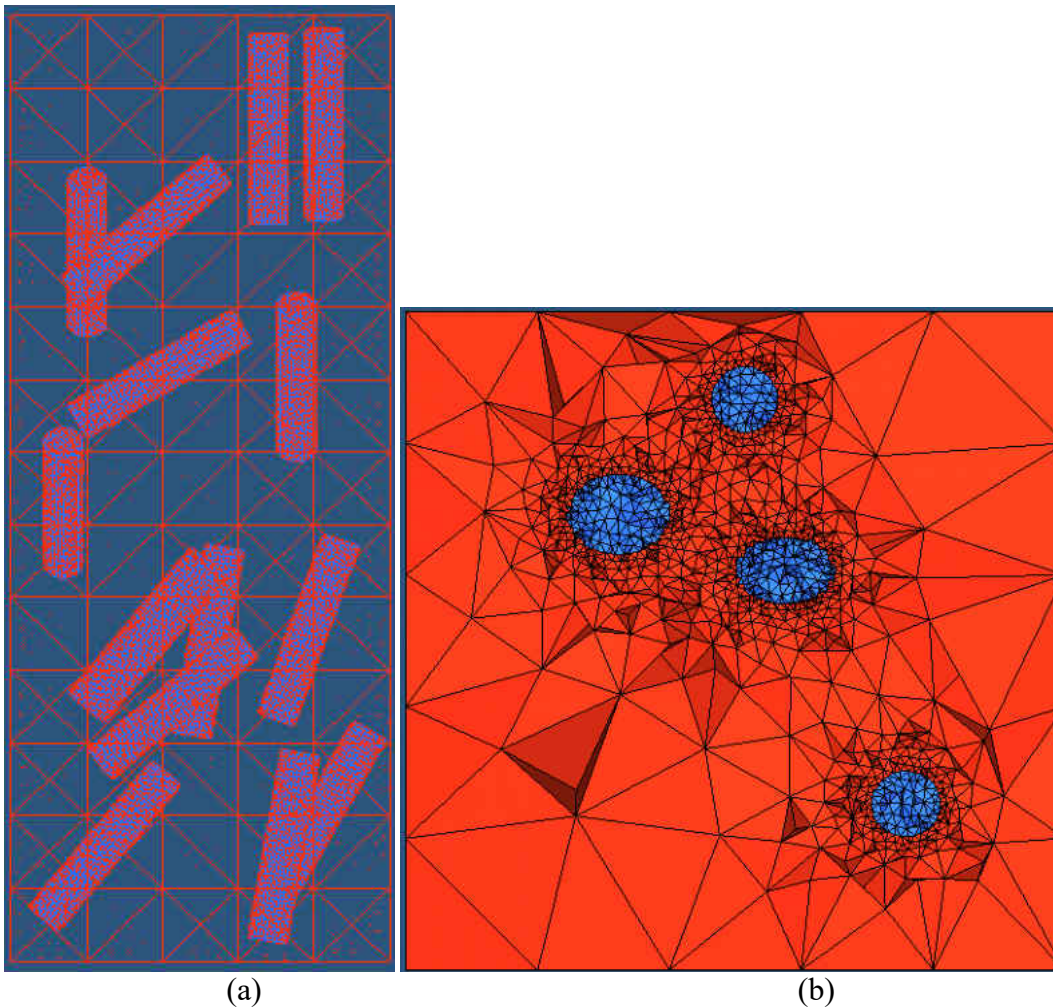
Figure 36 3D CNT composite finite element model

6.3 3D Cu/CNT composite model calculation & discussion

The CNT materials properties is obtained from two wall CNT H/D=9.1, as listed in Table 7. With the boundary conditions imposed, which are presented in

Table 9, on 3D unit cell models, calculation result is obtained.

To validate the model, we built a model in which all the materials are all copper. The comparison of models with tetra elements calculation results with experiment result is showed in Figure 37. In the calculation result that is showed in Figure 37, we have to double the engineering stress of calculation result, which is the only way to match the calculation result with experiment result. This is a "bug" in LS-DYNA (ls971_d_R5.1.1_winx64_p.exe) in terms of calculating reaction forces.
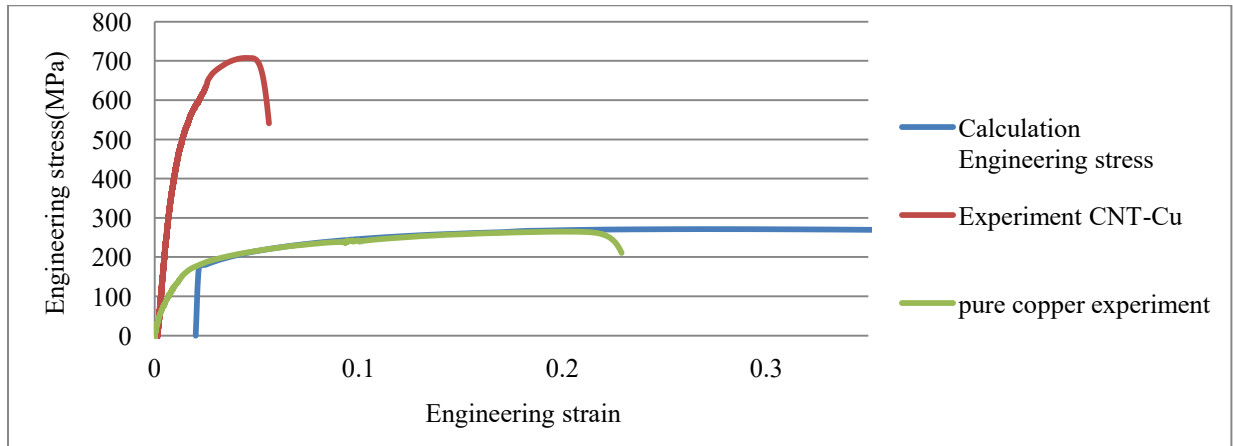
Figure 37 3D copper unit cell model calculation result & experiment result
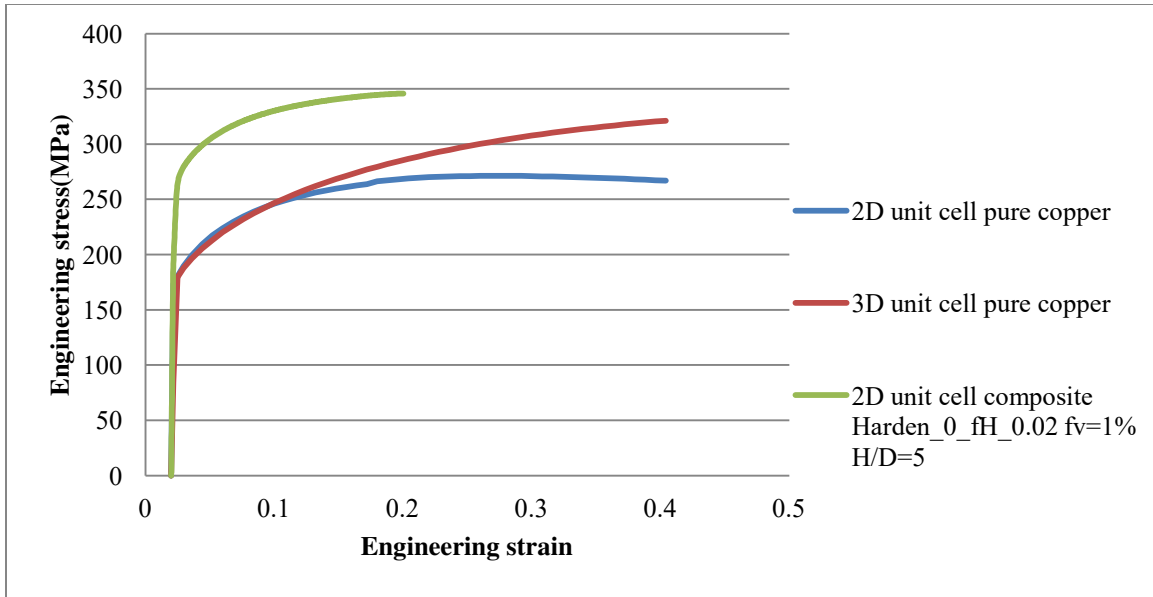
Figure 38 2D unit cell model & 3D unit cell model comparison

Comparison between 3D unit cell and 2D unit cell model is presented in Figure 38, 2D unit cell model is constructed without harden strain. The volume fraction of 2D unit cell is about 1%, and the volume fraction of 3D unit cell is about 2%. Stress value of 3D unit cell is doubled according to simulation result in Figure 37. Figure 38 shows that CNT in 3D models play very slight role in reinforcing composite material; there is slight different between 3D CNT composite unit cell model and 2D unit cell model with pure copper. The reason is due to the orientation of CNTs.

In this chapter, we developed a 3D unit cell model to simulate composite material behavior, but unfortunately the calculation result is neither match experiment nor 2D unit cell model result. Further research should be performed to on resolve this incorrect simulation, and to develop ways to impose residual stress around CNT in 3D unit cell composites models.

CHAPTER 7 CONCLUSION

In this thesis, we develop FEA model to simulate Cu/CNT composite material, and study possible hardening mechanisms of CNT to reinforce copper. We have studied the method to build up 2D and 3D unit model to study Cu/CNT composite hardness and failure mechanism under complex stress conditions, and built up a feasible model to predict composite materials behavior.

1. Our research shows that to reduce mesh size effect, nonlocal material method can reduce some mesh size effect on FEA calculation, but it cannot fully solve mesh size effect.

2. In our research, we tried to build up a unit cell model which comes with linear constrain boundary. Our calculations show that several factors can affect simulation result greatly. These factors include: CNT volume fraction, harden strain, hardened region volume fraction, model aspect ratio and meshes size.

3. In our research we did a series of calculation with different CNT volume fraction; harden strain, hardened region volume fraction, model aspect ratio. Our simulation shows that hardness of Cu/CNT composites model increases monotonically with CNT volume fraction, harden strain and hardened region volume fraction. For the aspect ratio, we found when H/D=1, the yield stress of Cu/CNT models reaches its minimum value as showed in Figure 30. Yield stress increases when H/D>1 or H/D<1. Our research is only focused in h/D≥1, which is a monotonically increasing range. The yield stress of Cu/CNT composite model

does not change much after H/D≈10, so we choose MD simulation result of H/D=9.1(which is presented in [12]) as our uniform CNT properties.

4. Based on the current research, there are three possible mechanisms that can change copper hardness: residual stress[17], strain gradient[154] and size dependence[155]; Because of the limitation of time, we focus our research on residual stress which is generated during composite material manufacture process. Further research is needed to study the other two factors.

REFERENCES

1. Iijima, S., *Helical microtubules of graphitic carbon.* Nature, 1991. **354**(6348): p. 56-58.
2. Iijima, S. and T. Ichihashi, *Single-shell carbon nanotubes of 1-nm diameter.* Nature, 1993. **363**(6430): p. 603-605.
3. Bethune, D.S., et al., *Cobalt-catalysed growth of carbon nanotubes with single-atomic-layer walls.* Nature, 1993. **363**(6430): p. 605-607.
4. Byengsoo, L., et al., *The effects of interfacial bonding on mechanical properties of single-walled carbon nanotube reinforced copper matrix nanocomposites.* Nanotechnology, 2006. **17**(23): p. 5759.
5. Cha, S.I., et al., *Extraordinary Strengthening Effect of Carbon Nanotubes in Metal-Matrix Nanocomposites Processed by Molecular-Level Mixing.* Advanced Materials, 2005. **17**(11): p. 1377-1381.
6. Chen, W.X., et al., *Tribological application of carbon nanotubes in a metal-based composite coating and composites.* Carbon, 2003. **41**(2): p. 215-222.
7. Zhan, G.-D., et al., *Single-wall carbon nanotubes as attractive toughening agents in alumina-based nanocomposites.* Nat Mater, 2003. **2**(1): p. 38-42.
8. Graff, R.A., et al., *Achieving Individual-Nanotube Dispersion at High Loading in Single-Walled Carbon Nanotube Composites (Adv. Mater. 2005, 8, 980).* Advanced Materials, 2005. **17**(15): p. 1820-1820.
9. Llorca, J., A. Needleman, and S. Suresh, *An analysis of the effects of matrix void growth on deformation and ductility in metal-ceramic composites.* Acta Metallurgica et Materialia, 1991. **39**(10): p. 2317-2335.
10. Xiao, J.R., B.A. Gama, and J.W. Gillespie Jr, *An analytical molecular structural mechanics model for the mechanical properties of carbon nanotubes.* International Journal of Solids and Structures, 2005. **42**(11-12): p. 3075-3092.
11. Frankland, S.J.V., et al., *The stress-strain behavior of polymer-nanotube composites from molecular dynamics simulation.* Composites Science and Technology, 2003. **63**(11): p. 1655-1661.
12. Liew, K.M., X.Q. He, and C.H. Wong, *On the study of elastic and plastic properties of multi-walled carbon nanotubes under axial tension using molecular dynamics simulation.* Acta Materialia, 2004. **52**(9): p. 2521-2527.
13. Alex A. Volinsky, M.H., Joseph B. Vella, N.V. Edwards, Rich Gregory, William W. Gerberich, *Residual Stress and Microstructure of Electroplated Cu Film on Different Barrier Layers.* MRS Proceedings, 2002. **695**: p. 6.
14. Dai, L.H., Z. Ling, and Y.L. Bai, *Size-dependent inelastic behavior of particle-reinforced metal-matrix composites.* Composites Science and Technology, 2001. **61**(8): p. 1057-1063.
15. Kandil, F.A., et al., *A review of residual stress measurement methods - a guide to technique selection.* NPL Report MATC(A)04, 2001.
16. Shao, J.C., et al., *An enhanced FEM model for particle size dependent flow strengthening and interface damage in particle reinforced metal matrix composites.* Composites Science and Technology. **71**(1): p. 39-45.
17. Suh, Y.S., S.P. Joshi, and K.T. Ramesh, *An enhanced continuum model for size-dependent strengthening and failure of particle-reinforced composites.* Acta Materialia, 2009. **57**(19): p. 5848-5861.
18. Ls-DYNA, *Keyword User's Manual.* 2007. **Volumes I and II**: p. 1.

19. Pijaudier-Cabot, G. and Z.P. Bazant, *Nonlocal Damage Theory.* Journal of Engineering Mechanics, 1987. **113**(10): p. 1512-1533.

20. *Helical microtubules of graphite carbon.* Nature, 1991. **354**(6348): p. 56.

21. *Single-shell carbon nanotubes of 1 nm diameter.* Nature, 1993. **363**(6430): p. 603.

22. *Cobalt-catalyzed growth of carbon nanotubes with single atomic-layer walls.* Nature, 1993. **363**(6430): p. 605.

23. Jia, Z., et al., *Study on poly(methyl methacrylate)/carbon nanotube composites.* Materials Science and Engineering: A, 1999. **271**(1-2): p. 395-400.

24. Shaffer, M.S.P. and A.H. Windle, *Fabrication and Characterization of Carbon Nanotube/Poly(vinyl alcohol) Composites.* Advanced Materials, 1999. **11**(11): p. 937-941.

25. Ledwith, D.M., A.M. Whelan, and J.M. Kelly, *A rapid, straight-forward method for controlling the morphology of stable silver nanoparticles.* Journal of Materials Chemistry, 2007. **17**(23).

26. Rawal, S., *Metal-matrix composites for space applications.* JOM Journal of the Minerals, Metals and Materials Society, 2001. **53**(4): p. 14-17.

27. Shelley, J., R. LeClaire, and J. Nichols, *Metal-matrix composites for liquid rocket engines.* JOM Journal of the Minerals, Metals and Materials Society, 2001. **53**(4): p. 18-21.

28. Yu, M.-F., et al., *Tensile Loading of Ropes of Single Wall Carbon Nanotubes and their Mechanical Properties.* Physical Review Letters, 2000. **84**(24): p. 5552-5555.

29. Yu, M.-F., et al., *Strength and Breaking Mechanism of Multiwalled Carbon Nanotubes Under Tensile Load.* Science, 2000. **287**(5453): p. 637-640.

30. Wong, E.W., P.E. Sheehan, and C.M. Lieber, *Nanobeam Mechanics: Elasticity, Strength, and Toughness of Nanorods and Nanotubes.* Science, 1997. **277**(5334): p. 1971-1975.

31. Treacy, M.M.J., T.W. Ebbesen, and J.M. Gibson, *Exceptionally high Young's modulus observed for individual carbon nanotubes.* Nature, 1996. **381**(6584): p. 678-680.

32. Yakobson, B.I., C.J. Brabec, and J. Bernholc, *Nanomechanics of Carbon Tubes: Instabilities beyond Linear Response.* Physical Review Letters, 1996. **76**(14): p. 2511-2514.

33. Lu, J.P., *Elastic Properties of Carbon Nanotubes and Nanoropes.* Physical Review Letters, 1997. **79**(7): p. 1297-1300.

34. *Elastic strain of freely suspended single-wall carbon nanotube ropes.* Appl. Phys. Lett., 1999. **74**(25): p. 3803.

35. Wagner, H.D., et al., *Stress-induced fragmentation of multiwall carbon nanotubes in a polymer matrix.* Applied Physics Letters, 1998. **72**(2): p. 188-190.

36. *Atomistic simulation of nanotube fracture.* Phys. Rev., 2002. **65**(23): p. 235430.

37. *Structural flexibility of carbon nanotubes.* J. Chem. Phys., 1996. **104**(5): p. 2089.

38. Berber, S., Y.-K. Kwon, and D. Tománek, *Unusually High Thermal Conductivity of Carbon Nanotubes.* Physical Review Letters, 2000. **84**(20): p. 4613-4616.

39. Kim, P., et al., *Thermal Transport Measurements of Individual Multiwalled Nanotubes.* Physical Review Letters, 2001. **87**(21): p. 215502.

40. Abu Bakar Sulong, J.P., *Alignment of multi-walled carbon nanotubes in a polyethylene matrix by extrusion shear flow: mechanical properties enhancement.* Journal of Composite Materials, 2010. **45**: p. 11.

41. Bakshi, S.R., D. Lahiri, and A. Agarwal, *Carbon nanotube reinforced metal matrix composites - a review.* International Materials Reviews. **55**(1): p. 41-64.

42. Ishikawa, T., *Overview of trends in advanced composite research and applications in Japan.* Review Literature And Arts Of The Americas 2006. **15**(1): p. 35.

43.   Coleman, J.N., et al., *Small but strong: A review of the mechanical properties of carbon nanotube-polymer composites.* Carbon, 2006. **44**(9): p. 1624-1652.

44.   Liliane, B., *Multiwall carbon nanotube elastomeric composites: A review.* Polymer, 2007. **48**(17): p. 4907-4920.

45.   Regev, O., et al., *Preparation of Conductive Nanotube–Polymer Composites Using Latex Technology.* Advanced Materials, 2004. **16**(3): p. 248-251.

46.   Bower, C., et al., *Deformation of carbon nanotubes in nanotube--polymer composites.* Applied Physics Letters, 1999. **74**(22): p. 3317-3319.

47.   Andrews, R., et al., *Nanotube composite carbon fibers.* Applied Physics Letters, 1999. **75**(9): p. 1329-1331.

48.   Haggenmueller, R., et al., *Aligned single-wall carbon nanotubes in composites by melt processing methods.* Chemical Physics Letters, 2000. **330**(3-4): p. 219-225.

49.   Allaoui, A., et al., *Mechanical and electrical properties of a MWNT/epoxy composite.* Composites Science and Technology, 2002. **62**(15): p. 1993-1998.

50.   Lau, K.-t., S.-Q. Shi, and H.-m. Cheng, *Micro-mechanical properties and morphological observation on fracture surfaces of carbon nanotube composites pre-treated at different temperatures.* Composites Science and Technology, 2003. **63**(8): p. 1161-1164.

51.   Peigney, A., et al., *Carbon nanotubes in novel ceramic matrix nanocomposites.* Ceramics International, 2000. **26**(6): p. 677-683.

52.   Curtin, W.A. and B.W. Sheldon, *CNT-reinforced ceramics and metals.* Materials Today, 2004. **7**(11): p. 44-49.

53.   White, A.A., S.M. Best, and I.A. Kinloch, *Hydroxyapatite–Carbon Nanotube Composites for Biomedical Applications: A Review.* International Journal of Applied Ceramic Technology, 2007. **4**(1): p. 1-13.

54.   Jin, L., C. Bower, and O. Zhou, *Alignment of carbon nanotubes in a polymer matrix by mechanical stretching.* Applied Physics Letters, 1998. **73**(9): p. 1197-1199.

55.   Tu, J.P., et al., *Tribological properties of carbon-nanotube-reinforced copper composites.* Tribology Letters, 2001. **10**(4): p. 225-228.

56.   He, C., et al., *An Approach to Obtaining Homogeneously Dispersed Carbon Nanotubes in Al Powders for Preparing Reinforced Al-Matrix Composites.* Advanced Materials, 2007. **19**(8): p. 1128-1132.

57.   Shi, X.L., et al., *Fabrication and properties of W-Cu alloy reinforced by multi-walled carbon nanotubes.* Materials Science and Engineering: A, 2007. **457**(1-2): p. 18-23.

58.   Feng, Y., H.L. Yuan, and M. Zhang, *Fabrication and properties of silver-matrix composites reinforced by carbon nanotubes.* Materials Characterization, 2005. **55**(3): p. 211-218.

59.   Xu, C.L., et al., *Fabrication of aluminum-carbon nanotube composites and their electrical properties.* Carbon, 1999. **37**(5): p. 855-858.

60.   Zhong, R., H. Cong, and P. Hou, *Fabrication of nano-Al based composites reinforced by single-walled carbon nanotubes.* Carbon, 2003. **41**(4): p. 848-851.

61.   Deng, C.F., et al., *Calorimetric study of carbon nanotubes and aluminum.* Materials Letters, 2007. **61**(14-15): p. 3221-3223.

62.   Kuzumaki, T., et al., *Mechanical Characteristics and Preparation of Carbon Nanotube Fiber-Reinforced Ti Composite.* Advanced Engineering Materials, 2000. **2**(7): p. 416-418.

63.   Carreño-Morelli, E., et al., *Carbon nanotube/magnesium composites.* physica status solidi (a), 2004. **201**(8): p. R53-R55.

64. Pang, L.X., et al., *Microstructure, Hardness, and Bending Strength of Carbon Nanotube-Iron Aluminide Composites.* Journal of Composite Materials, 2007. **41**(16): p. 2025-2031.

65. Hulbert, D.M., et al., *A discussion on the absence of plasma in spark plasma sintering.* Scripta Materialia, 2009. **60**(10): p. 835-838.

66. Kim, K.T., et al., *Microstructures and tensile behavior of carbon nanotube reinforced Cu matrix nanocomposites.* Materials Science and Engineering: A, 2006. **430**(1-2): p. 27-33.

67. Kim, K.T., S.I. Cha, and S.H. Hong, *Hardness and wear resistance of carbon nanotube reinforced Cu matrix nanocomposites.* Materials Science and Engineering: A, 2007. **449-451**(0): p. 46-50.

68. Kwon, H., et al., *Combination of hot extrusion and spark plasma sintering for producing carbon nanotube reinforced aluminum matrix composites.* Carbon, 2009. **47**(3): p. 570-577.

69. Kuzumaki, T., et al., *Processing of Carbon Nanotube Reinforced Aluminum Composite.* Journal of Materials Research, 1998. **13**(09): p. 5.

70. Quang, P., et al., *Equal Channel Angular Pressing of Carbon Nanotube Reinforced Metal Matrix Nanocomposites.* Key Engineering Materials 2006. **326-328**: p. 4.

71. Quang, P., et al., *Consolidation of 1 vol.% carbon nanotube reinforced metal matrix nanocomposites via equal channel angular pressing.* Journal of Materials Processing Technology, 2007. **187-188**(0): p. 318-320.

72. Dong, S.R., J.P. Tu, and X.B. Zhang, *An investigation of the sliding wear behavior of Cu-matrix composite reinforced by carbon nanotubes.* Materials Science and Engineering: A, 2001. **313**(1-2): p. 83-87.

73. George, R., et al., *Strengthening in carbon nanotube/aluminium (CNT/Al) composites.* Scripta Materialia, 2005. **53**(10): p. 1159-1163.

74. Deng, C.F., et al., *Processing and properties of carbon nanotubes reinforced aluminum composites.* Materials Science and Engineering: A, 2007. **444**(1-2): p. 138-145.

75. Deng, C., et al., *Fabrication of aluminum matrix composite reinforced with carbon nanotubes.* Rare Metals, 2007. **26**(5): p. 450-455.

76. Deng, C., et al., *Preparation and characterization of carbon nanotubes/aluminum matrix composites.* Materials Letters, 2007. **61**(8-9): p. 1725-1728.

77. Deng, C.F., et al., *Thermal expansion behaviors of aluminum composite reinforced with carbon nanotubes.* Materials Letters, 2008. **62**(15): p. 2301-2303.

78. Esawi, A.M.K. and M.A. El Borady, *Carbon nanotube-reinforced aluminium strips.* Composites Science and Technology, 2008. **68**(2): p. 486-492.

79. Choi, H.J., et al., *Reinforcement with carbon nanotubes in aluminum matrix composites.* Scripta Materialia, 2008. **59**(3): p. 360-363.

80. Zan, B., et al., *Carbon-nanotube-reinforced $Zr_{52.5}Cu_{17.9}Ni_{14.6}Al_{10}Ti_5$ bulk metallic glass composites.* Applied Physics Letters, 2002. **81**(25): p. 4739-4741.

81. Bian, Z., et al., *Carbon-Nanotube-Reinforced Zr-Based Bulk Metallic Glass Composites and Their Properties.* Advanced Functional Materials, 2004. **14**(1): p. 55-63.

82. Goh, C.S., et al., *Simultaneous enhancement in strength and ductility by reinforcing magnesium with carbon nanotubes.* Materials Science and Engineering: A, 2006. **423**(1-2): p. 153-156.

83. Goh, C.S., et al., *Ductility improvement and fatigue studies in Mg-CNT nanocomposites.* Composites Science and Technology, 2008. **68**(6): p. 1432-1439.

84. Yang, J. and R. Schaller, *Mechanical spectroscopy of Mg reinforced with Al_2O_3 short fibers and C nanotubes.* Materials Science and Engineering: A, 2004. **370**(1-2): p. 512-515.

85. Zhou, S.-m., et al., *Fabrication and tribological properties of carbon nanotubes reinforced Al composites prepared by pressureless infiltration technique.* Composites Part A: Applied Science and Manufacturing, 2007. **38**(2): p. 301-306.

86. Li, Y.B., et al., *Processing of a carbon nanotubes--Fe$_{82}$P$_{18}$ metallic glass composite.* Journal of Materials Science Letters, 1998. **17**(7): p. 607-609.

87. Hwang, J.Y., et al., *Laser-deposited carbon nanotube reinforced nickel matrix composites.* Scripta Materialia, 2008. **59**(5): p. 487-490.

88. Yang, Y.L., et al., *Single-walled carbon nanotube-reinforced copper composite coatings prepared by electrodeposition under ultrasonic field.* Materials Letters, 2008. **62**(1): p. 47-50.

89. Arai, S., M. Endo, and N. Kaneko, *Ni-deposited multi-walled carbon nanotubes by electrodeposition.* Carbon, 2004. **42**(3): p. 641-644.

90. Arai, S., et al., *Excellent solid lubrication of electrodeposited nickel-multiwalled carbon nanotube composite films.* Materials Letters, 2008. **62**(20): p. 3545-3548.

91. Chen, X.H., et al., *Corrosion behavior of carbon nanotubes-Ni composite coating.* Surface and Coatings Technology, 2005. **191**(2-3): p. 351-356.

92. Chen, X.H., et al., *Electrodeposited nickel composites containing carbon nanotubes.* Surface and Coatings Technology, 2002. **155**(2-3): p. 274-278.

93. Chen, X.H., et al., *Tribological behavior of carbon nanotubes—reinforced nickel matrix composite coatings.* Journal of Materials Science Letters, 2001. **20**(22): p. 2057-2060.

94. Shi, Y.L., et al., *Electroplated synthesis of Ni-P-UFD, Ni-P-CNTs, and Ni-P-UFD-CNTs composite coatings as hydrogen evolution electrodes.* Materials Chemistry and Physics, 2004. **87**(1): p. 154-161.

95. Tan, J., et al., *Microstructure and wear resistance of nickel–carbon nanotube composite coating from brush plating technique.* Tribology Letters, 2006. **21**(2): p. 107-111.

96. Xu, Q., L. Zhang, and J. Zhu, *Controlled Growth of Composite Nanowires Based on Coating Ni on Carbon Nanotubes by Electrochemical Deposition Method.* The Journal of Physical Chemistry B, 2003. **107**(33): p. 8294-8296.

97. Arai, S., et al., *Fabrication of Nickel--Multiwalled Carbon Nanotube Composite Films with Excellent Thermal Conductivity by an Electrodeposition Technique.* Electrochemical and Solid-State Letters, 2006. **9**(8): p. C131-C133.

98. Shi, L., et al., *Electrodeposition and characterization of Ni-Co-Carbon nanotubes composite coatings.* Surface and Coatings Technology, 2006. **200**(16-17): p. 4870-4875.

99. Susumu, A., S. Takashi, and E. Morinobu, *Low-Internal-Stress Nickel Multiwalled Carbon Nanotube Composite Electrodeposited from a Sulfamate Bath.* Journal of The Electrochemical Society, 2007. **154**(10): p. D530-D533.

100. Guo, C., et al., *The effects of pulse-reverse parameters on the properties of Ni-carbon nanotubes composite coatings.* Surface and Coatings Technology, 2007. **201**(24): p. 9491-9496.

101. Guo, C., et al., *The effects of electrodeposition current density on properties of Ni-CNTs composite coatings.* Surface and Coatings Technology, 2008. **202**(14): p. 3246-3250.

102. Dai, P.-Q., W.-C. Xu, and Q.-Y. Huang, *Mechanical properties and microstructure of nanocrystalline nickel-carbon nanotube composites produced by electrodeposition.* Materials Science and Engineering: A, 2008. **483-484**(0): p. 172-174.

103. Kang, X., et al., *A sensitive nonenzymatic glucose sensor in alkaline media with a copper nanocluster/multiwall carbon nanotube-modified glassy carbon electrode.* Analytical Biochemistry, 2007. **363**(1): p. 143-150.

104.   Yang, C., et al. *Carbon Nanotube/Copper Composites for Via Filling and Thermal Management*. in *Electronic Components and Technology Conference, 2007. ECTC '07. Proceedings. 57th*. 2007.

105.   Ferrer-Anglada, N., et al., *Carbon nanotube based composites for electronic applications: CNT–conducting polymers, CNT–Cu.* physica status solidi (a), 2006. **203**(6): p. 1082-1087.

106.   Ngo, Q., et al., *Thermal Interface Properties of Cu-filled Vertically Aligned Carbon Nanofiber Arrays.* Nano Letters, 2004. **4**(12): p. 2403-2407.

107.   Feng, X.M., X.P. Ai, and H.X. Yang, *A positive-temperature-coefficient electrode with thermal cut-off mechanism for use in rechargeable lithium batteries.* Electrochemistry Communications, 2004. **6**(10): p. 1021-1024.

108.   Chen, X.H., et al., *Dry friction and wear characteristics of nickel/carbon nanotube electroless composite deposits.* Tribology International, 2006. **39**(1): p. 22-28.

109.   Arai, S., et al., *Nickel-coated carbon nanofibers prepared by electroless deposition.* Electrochemistry Communications, 2004. **6**(10): p. 1029-1031.

110.   Susumu, A., et al., *Fabrication of Nickel--Multiwalled Carbon Nanotube Composite Films with Excellent Thermal Conductivity by an Electrodeposition Technique.* Electrochemical and Solid-State Letters, 2006. **9**(8): p. C131-C133.

111.   Shi, L., et al., *Electrodeposition and characterization of Ni-Co-Carbon nanotube somposite coatings.* Surface and Coatings Technology, 2006. **200**(16-17): p. 4870-4875.

112.   Susumu, A., S. Yoriyuki, and E. Morinobu, *Cu/Multiwalled Carbon Nanotube Composite Films Fabricated by Pulse-Reverse Electrodeposition.* Journal of The Electrochemical Society. **158**(2): p. D49-D53.

113.   Chen, X., et al., *Carbon-nanotube metal-matrix composites prepared by electroless plating.* Composites Science and Technology, 2000. **60**(2): p. 301-306.

114.   Yucheng, W., et al., *Preparation and characterization of Ni-Cu-P/CNTs quaternary electroless composite coating.* Materials Research Bulletin, 2008. **43**(12): p. 3425-3432.

115.   Fauchais, P., A. Vardelle, and B. Dussoubs, *Quo Vadis thermal spraying?* Journal of Thermal Spray Technology, 2001. **10**(1): p. 44-66.

116.   Meyer, W., *Metal spraying in the United States: A jtst historical paper.* Journal of Thermal Spray Technology, 1996. **5**(1): p. 79-83.

117.   Berndt, C. and E. Lavernia, *Thermal spray processing of nanoscale materials—A conference report with extended abstract.* Journal of Thermal Spray Technology, 1998. **7**(3): p. 411-440.

118.   Ping, C., et al., *Preparation of Cu/CNT Composite Particles and Catalytic Performance on Thermal Decomposition of Ammonium Perchlorate.* Propellants, Explosives, Pyrotechnics, 2006. **31**(6): p. 452-455.

119.   Kim, K.T., et al., *The Role of Interfacial Oxygen Atoms in the Enhanced Mechanical Properties of Carbon-Nanotube-Reinforced Metal Matrix Nanocomposites.* Small, 2008. **4**(11): p. 1936-1940.

120.   Huang, W., H. Chen, and J.-M. Zuo, *One-Dimensional Self-Assembly of Metallic Nanostructures on Single-Walled Carbon-Nanotube Bundles.* Small, 2006. **2**(12): p. 1418-1421.

121.   Ci, L., et al., *Investigation of the interfacial reaction between multi-walled carbon nanotubes and aluminum.* Acta Materialia, 2006. **54**(20): p. 5367-5375.

122.   Borino, G., B. Failla, and F. Parrinello, *A symmetric nonlocal damage theory.* International Journal of Solids and Structures, 2003. **40**(13-14): p. 3621-3645.

123.   Bažant, Z. and B. Oh, *Crack band theory for fracture of concrete.* Materials and Structures, 1983. **16**(3): p. 155-177.

124. Etse, G. and K. Willam, *Fracture Energy Formulation for Inelastic Behavior of Plain Concrete.* Journal of Engineering Mechanics, 1994. **120**(9): p. 1983-2011.

125. Comi, C. and U. Perego, *Fracture energy based bi-dissipative damage model for concrete.* International Journal of Solids and Structures, 2001. **38**(36-37): p. 6427-6454.

126. A.Cemal, E., *On nonlocal plasticity.* International Journal of Engineering Science, 1981. **19**(12): p. 1461-1474.

127. Gilles, P.-C. and P.B. Zdenek, *Nonlocal Damage Theory.* Journal of Engineering Mechanics, 1987. **113**(10): p. 1512-1533.

128. Borino, G., P. Fuschi, and C. Polizzotto, *A Thermodynamic Approach to Nonlocal Plasticity and Related Variational Principles.* Journal of Applied Mechanics, 1999. **66**(4): p. 952-963.

129. Ganghoffer, J.F., L.J. Sluys, and R. de Borst, *A reappraisal of nonlocal mechanics.* European Journal of Mechanics - A/Solids. **18**(1): p. 17-46.

130. Aifantis, E.C., *On the Microstructural Origin of Certain Inelastic Models.* Journal of Engineering Materials and Technology, 1984. **106**(4): p. 326-330.

131. Elias C, A., *On the role of gradients in the localization of deformation and fracture.* International Journal of Engineering Science, 1992. **30**(10): p. 1279-1299.

132. De Borst, R. and H.-B. Mühlhaus, *Gradient-dependent plasticity: Formulation and algorithmic aspects.* International Journal for Numerical Methods in Engineering, 1992. **35**(3): p. 521-539.

133. Borst, R.d. and J. Pamin, *Gradient plasticity in numerical simulation of concrete cracking.* European journal of mechanics, 1996. **15**(2): p. 2.

134. Addessi, D., S. Marfia, and E. Sacco, *A plastic nonlocal damage model.* Computer Methods in Applied Mechanics and Engineering, 2002. **191**(13-14): p. 1291-1310.

135. Polizzotto, C., G. Borino, and P. Fuschi, *A thermodynamically consistent formulation of nonlocal and gradient plasticity.* Mechanics Research Communications. **25**(1): p. 75-82.

136. Benvenuti, E., G. Borino, and A. Tralli, *A thermodynamically consistent nonlocal formulation for damaging materials.* European Journal of Mechanics - A/Solids, 2002. **21**(4): p. 535-553.

137. Sicot, O., et al., *Determination of Residual Stress in Composite Laminates Using the Incremental Hole-drilling Method.* Journal of Composite Materials, 2003. **37**(9): p. 831-844.

138. Arsenault, R.J. and N. Shi, *Dislocation generation due to differences between the coefficients of thermal expansion.* Materials Science and Engineering, 1986. **81**: p. 13.

139. Qu, S., et al., *A study of particle size effect and interface fracture in aluminum alloy composite via an extended conventional theory of mechanism-based strain-gradient plasticity.* Composites Science and Technology, 2005. **65**(7-8): p. 1244-1253.

140. Xue, Z., Y. Huang, and M. Li, *Particle size effect in metallic materials: a study by the theory of mechanism-based strain gradient plasticity.* Acta Materialia, 2002. **50**(1): p. 149-160.

141. Rozeveld, S.J., J.M. Howe, and S. Schmauder, *Measurement of residual strain in An AlSiCw composite using convergent-beam electron diffraction.* Acta Metallurgica et Materialia, 1992. **40, Supplement**(0): p. S173-S193.

142. Yin, W., N.M. Strickland, and P.G. Ifju, *Residual Strain Measurement and Residual Stress Prediction of Woven Composites.* Proceedings of the XIth International Congress and Exposition, 2008.

143. Zhu, W., L. Jian, and H. Bongtae, *Study of Residual Stress Distribution by a Combined Method of Moir[e-acute] Interferometry and Incremental Hole Drilling, Part I: Theory.* Journal of Applied Mechanics, 1998. **65**(4): p. 837-843.

144. Benedikt, B., et al., *Determination of Interlaminar Residual Thermal Stresses in a Woven 8HS Graphite/PMR-15 Composite Using X-Ray Diffraction Measurements.* Mechanics of Advanced Materials and Structures, 2002. **9**(4): p. 375-394.

145. Zewi, I., I. Daniel, and J. Gotro, *Residual stresses and warpage in woven-glass/epoxy laminates.* Experimental Mechanics, 1987. **27**(1): p. 44-50.

146. Huang, X., J.W. Gillespie Jr, and T. Bogetti, *Process induced stress for woven fabric thick section composite structures.* Composite Structures, 2000. **49**(3): p. 303-312.

147. Guangyu, C., et al., *Mechanical properties of carbon nanotube-copper nanocomposites.* Journal of Micromechanics and Microengineering, 2008. **18**(3): p. 035013.

148. Lau, A.K.-T. and D. Hui, *The revolutionary creation of new advanced materials- carbon nanotube composites.* Composites Part B: Engineering, 2002. **33**(4): p. 263-277.

149. Lau, K.-T. and D. Hui, *Effectiveness of using carbon nanotubes as nano-reinforcements for advanced composite structures.* Carbon, 2002. **40**(9): p. 1605-1606.

150. Guangyu, C., et al., *Mechanical properties of carbon nanotube-copper nanocomposites.* Journal of Micromechanics and Microengineering, 2008. **18**(3): p. 035013.

151. wikipedia, *http://en.wikipedia.org/wiki/Copper.*

152. Zhang, P., P.E. Lammert, and V.H. Crespi, *Plastic Deformations of Carbon Nanotubes.* Physical Review Letters, 1998. **81**(24): p. 5346-5349.

153. Lu, Q., et al., *Determination of Carbon Nanotube Density by Gradient Sedimentation.* The Journal of Physical Chemistry B, 2006. **110**(48): p. 24371-24376.

154. Fleck, N.A., et al., *Strain gradient plasticity: Theory and experiment.* Acta Metallurgica et Materialia, 1994. **42**(2): p. 475-487.

155. Fredriksson, P. and P. Gudmundson, *Size-dependent yield strength of thin films.* International Journal of Plasticity, 2005. **21**(9): p. 1834-1854.